Ca' Foscari
University
of Venice

Master's Degree programme

in

Conservation Science and Technology for
Cultural Heritage

Final Thesis

Soil characterisation to investigate the role of burial environment in archaeological glass alteration

Supervisor
Ch. Prof. Dario Battistel

Assistant supervisor
Dr. Arianna Traviglia (CCHT@CaFoscari)

Graduand
Sofia Toniolo
Matriculation Number 862756

Academic Year
2020 / 2021

To my family

ABSTRACT

This thesis project is focused on the direct interactions between ancient glass objects and the soils where they were buried. The thesis aims to clarify the mechanisms of ancient glass alteration. The physico-chemical properties as well as the alteration patinas of Roman glasses found in the archaeological site of Aquileia (North of Italy) were investigated through Optical and Scanning Electron Microscopy (SEM-EDS) and Laser Ablation Inductively Coupled Plasma Mass Spectrometry (LA-ICP-MS). On parallel, the chemistry and the physical properties of the environmental soils, corresponding to the site of the archaeological findings, were studied in terms of elemental composition, through Microwave Plasma Atomic Emission Spectroscopy (MP-AES), and characterised through ion-exchange capacity, conductivity and pH measurements.

Archaeological glass fragments developed alteration patterns – mainly pitting and iridescence, as well as discolouration – consistent with the centuries-long placement in burial environment. Specifically, the soil parameters considered with the intrinsic features of glasses explain the formation of different degradation marks on glass surface. The composition, the pH level of the soil and the cation exchange capacity resulted crucial in glass degradation. In particular, the glass samples with the highest degree of deterioration are associated to environmental soils characterised by low pH values and high cation exchange capacities.

CONTENTS

AIMS OF THE THESIS PROJECT

Glass objects have been produced since 2500 BC or even before [7,23]. Therefore, a huge quantity of archaeological findings is made of glass. Although our everyday experience warns that glass is fragile to mechanical stresses, glass is known to be a durable material. Common sense could point out that degradation agents acting on object surfaces exposed to the atmosphere do not hurt vitreous artefacts, even less if they reach us through soil, by which they seem to be preserved. Glass is a material as liable to alteration as other art materials. The reason why we generally consider it as a strong product is simply because we do not notice macroscopically the deteriorating processes affecting it.

This thesis is focused on the study of archaeological glasses and the influence of soil conditions to the surface degradation. Since the archaeological glass objects are usually found underground, showing different typologies of deterioration, the direct relationship between soil parameters and the resulting glass degradation is the main goal of this project. The research is divided into two parts: (i) I analysed the physicochemical characteristics of ancient glasses to identify alteration patinas formed on their surface; (ii) I considered the environmental soil where glass fragments were buried. In this second part, the study evaluated how the glass alteration is influenced by the chemistry of the soil. This research aims to be the forerunner of future studies and developments on this topic, as the scientific literature brings a huge quantity of information about soil analysis from the geological and agricultural point of view, but it is still lacking about the interactions between ancient glass alteration and soil. All the analytical methods will be discussed and selected according to the specific requirements. Despite the recent increasing interest on glass deterioration, scientific literature is gaunt in explaining how the environment modifies the properties of glasses. One peculiarity of this thesis project is the possibility to compare shared information with the direct study of original Roman glasses that have undergone burial conditions for centuries. The opportunity to sample the soils that preserved but also degraded glass fragments is an added value of this thesis. Therefore, I have a privileged point of view from which I can tend to achieve the primary objective, that is finding the interactions between ancient glass and soil, and at the same time, verify, confirm and/or add information to relevant literature about the mechanism of glass alteration.

During the pathway described by this thesis the glass material will be studied from a chemical point of view, inspecting its components and structures, to learn how degradation acts on it and why we should start considering soil as a weathering agent rather than a protective medium. Soil will be broken down to comprehend its compounds and its chemical properties. The ultimate target of this journey will be the discovering of the interactions between soil and archaeological glass.

This experimental study is focused on some archaeological glasses from the site of Aquileia (North of Italy) that present visible signs of degradation as well as the soils where they were found. Optical and Scanning Electron Microscopy (SEM-EDS) and Laser Ablation Inductively Coupled Plasma Mass Spectrometry (LA-ICP-MS) are used to observe and analyse glass surfaces. Soil samples are characterised and examined by means of Microwave Plasma Atomic Emission Spectroscopy (MP-AES) and through ion-exchange capacity, conductivity, and pH measurements.

1. INTRODUCTION

1.1. GLASS

The term "glass" refers to a solid material with a non-crystalline structure. Vitreous materials can be distinguished into four categories of products: glass, glaze, enamel, and faience, which are different in raw components and in manufacturing procedures. Besides glass, we can define glaze and enamel as thin glassy coating applied to the surface of ceramic and metallic products with the purpose to give waterproof properties and decorative features, respectively. Faience can be considered the precursor of common glass, since it is produced from similar raw materials that are not brought to molten, but to a typical temperature that allows to hold silica particles together [7].

Man-made glasses are obtained by heating silica (SiO_2) at high temperatures. At about 1700° C the crystal phase of silica melts and it is transformed into the corresponding liquid phase. The cooling process does not allow the crystal structure to form again, so the resulting material is amorphous. The reasons why this structure is formed can be understood better if we plot the temperature versus the specific volume (Figure 1). The raw material is under crystalline form and increasing the temperature it is transmuted into its liquid state once reached the melting point (T_f in the graph). Melted glass is characterised by high viscosity, which tends to increase during cooling, and it acquires such high values that the atoms are not able to reorganise themselves into a crystalline phase. Under a specific temperature, the transition point (T_g in the graph), the material shows its glassy state. In the light of this explanation, glass can be defined as "a material that can be cooled down below its supercooling range (that is, the temperature range between T_g and T_f) and reversibly heated above, without the appearance of crystalline phases" [7,19].

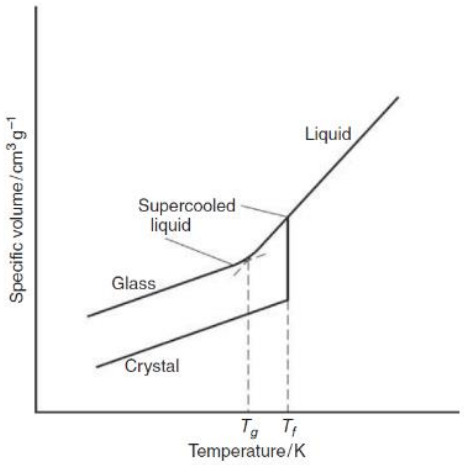

Figure 1. Graph from [19] showing temperature vs specific volume of silica. T_g is the transition point, T_f is the melting point.

The definition of glass according to its physico-chemical properties is not an action for its own sake, but it is the basis that allows us to understand how alteration agents act against the material.

1.1.1. THE STRUCTURE

Glass structure is not crystalline. At the atomic arrangement level, the atoms are linked together by bond forces in the range of those acting in crystals, and the elements present in higher amount build together a three-dimensional network. The difference with crystals is in the fact that the extended network is not periodical nor symmetrical, even if the energy content is the same. Therefore the structure of glass appears as a continuous network of tetrahedra arranged in a unregular order, forming a distorted structure [7,43].

The three-dimensional structure of man-made glass is given by silicon dioxide (SiO_2) organised in [SiO_4^{4-}] tetrahedra, where silicon occupies the centre of the structure and the oxygens are in the corners. The latter are shared with the adjacent tetrahedral units and provide the bridge between silicon atoms (Figure 2, left). The presence of alkali and alkaline-earth cations completes the internal configuration. As we can see in Figure 2, metal cations imply the breaking of tetrahedra bonds, developing non-bridging oxygens. The structure is therefore modified, and the properties of the glass are affected by the presence of alkali and alkaline-earth ions [7,19,43].

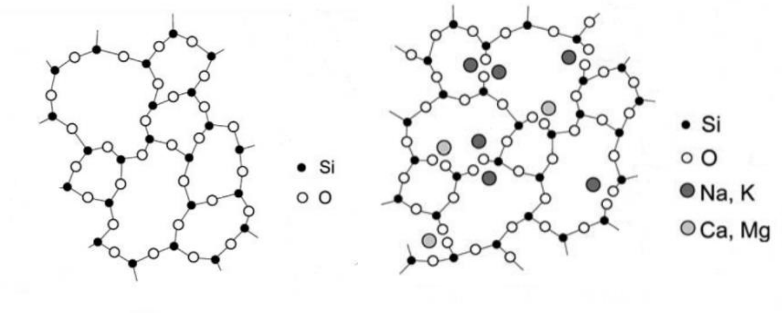

Figure 2. Two-dimensional representation of silica network (left) and structure modifications due to cations presence. Modified from [19].

The ingredients for the glass production recipe are different, depending on the time period and on the geographical place. Overall, they can be grouped according to the function they accomplish. As mentioned above, the main compound is silica, which is the vitrifier. Vitrifiers are stable oxides giving rise to the structure of the glass and, for this reason, they are also called *network formers*. The vitrifiers have high melting temperatures that, for working purposes, are lowered by fluxes, generally alkali-based compounds. Alkaline-earth oxides are added to increase glass stability and its resistance to water degradation. These two types of additives are called also *network modifiers*. Molten glass is homogenised and cleared from gas bubbles that can form during production processes though the use of fining agents. Aesthetic features linked to colour and transparency are reached with the addition of colourants and opacifiers [7,19].

The elements organised in the structure give peculiar optical and mechanical properties to the glass. Although the macroscopic features are as important as the microscopic ones in the understanding of the material behaviour during degradation events, the discussion will dwell on the composition and internal structure of glass, since alteration phenomena acting at small scales will be considered primarily.

1.1.2. RAW MATERIALS

The main sources of silicon dioxide in the past were quartz powder or the more used sand. The alkali components were natron or plant ashes. The former is a mineral deposit of sodium carbonate ($Na_2CO_3 \cdot NaHCO_3 \cdot 2H_2O$) coming from a dried lake in Egypt, whereas the latter were obtained from the burning of saltmarsh plants – rich in soda – or forest plants – with high amount of potash (K_2CO_3). The fluxes have been added to the batch to make the molten glass state easy to reach – as pure silica melts at about 1700° C – and to extend its workability, but an exceed of alkalis increases the water weakness of the glass. Lime (CaO), sometimes present as impurity in the sand used as silica source, stabilised the glass. Colour was brought by metal elements introduced as oxides, such as manganese (Mn^{3+}) or iron, able to give different shades according to the oxidation state (blue to green if Fe^{2+}, yellow to brown if Fe^{3+}) [19,21]. Instead, colourless glasses were obtained with the addition of manganese or antimony oxides to balance the iron presence as sand impurity, which gives green tints if oxidised (Fe^{2+}). Lots of other elements can be found in ancient glass artefacts since the raw materials were rarely pure and only during later period we were able to identify the precise elements needed to create these products [7].

1.1.3. ROMAN GLASS

The manufacture of glass achieved high technical levels in Roman times. The majority of vitreous artefacts were soda-lime-silica glasses, with siliceous sand and natron as main raw material. The amounts of magnesium and potassium in glass were low, generally with a concentration lower than 1.5%. The sand for glassmaking was probably from the eastern Mediterranean regions and it was low in iron content and high in purity, moreover it included a certain amount of lime, used as stabiliser. Additional calcium carbonate was added to the glass batch, reaching up to 5 to 10% of total content [7-8]. The typical composition of a Roman glass is reported in Table 1. The specific composition of Roman glasses makes the artifacts more durable to degradation than Medieval potash glasses [7].

Table 1. Typical composition of Roman glasses [7-8].

Oxide	*Amount in wt%*
SiO_2	70
Na_2O	15-20
CaO	5-10
Al_2O_3	2-3
MgO	<1
K_2O	<1

1.1.4. DETERIORATION OF GLASS

Studies about ancient glass deterioration originally started to answer questions regarding the visible decay of medieval stained windows. Afterwards, the recent and new application of glass as protection layer to incapsulate nuclear wastes gave a further stimulus [7,15,19,42].

For some reasons, not least the fact that the topic about glass degradation is little debated in conservation field, the terminology used in scientific literature is not coherent. Degradation phenomena affecting glass are named *corrosion*, even if this term is generally referred to metals decay [7,19,40]. With the term corrosion we include all glass deterioration events due to extrinsic and/or intrinsic factors. However the same word identifies the attacks by liquids, in opposition to *weathering*, that indicates the aggression by atmospheric agents and pollutants [7,19]. The latter is also used to identify the alteration in burial environments [40]. In order to be clear while discussing these topics, along this thesis the term corrosion will be used to indicate the attack of liquid to the glass, and weathering as glass deterioration due to atmospheric agents [19,29]. Alterations in burial environment will be mentioned with the term corrosion, as liquid water is involved in the phenomenon [13,42].

1.1.4.1. GLASS CORROSION MECHANISMS

Glass degradation is directly affected by the material composition and the environmental conditions. Concerning the internal structure of glasses, the different metal oxides, added as structural ingredients, modify the silica network. The interactions between network modifiers (M) and network formers provides the formation of terminal groups -Si-O-M or non-bridging oxygen atoms -Si-O-M-O-Si-, according to their monovalent or bivalent nature respectively, as reported in the scheme in Figure 3 [19]. The chemical structure is essential to understand the most common glass corrosion induced by water. In fact, water molecules have a higher affinity with metallic cations and non-bridging oxygens than Si-O-Si bonds, thus they dissociate and M-OH species are formed. Liquid water penetrates the glass by diffusion if voids are available or by hydrolysis reactions [13,42].

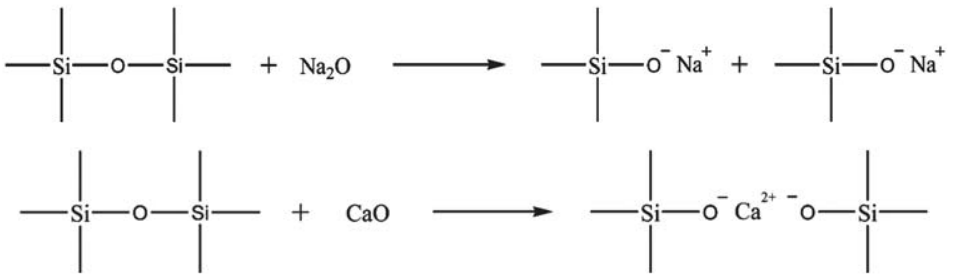

Figure 3. Interactions between network formers and network modifiers and the formation of terminal groups (top, with monovalent cations) or non-bridging oxygen atoms (bottom, with bivalent cations) [19].

Two fundamental mechanisms for glass corrosion are proposed [4,7,13,19,26,29,31,38]. The first mechanism, the stage 1 of corrosion shown in Figure 4, is an ion-exchange process involving the network modifiers. It happens in environmental contexts up to pH=9. The medium attacking the glass owns molecules and aggregates able to bear hydrogen ions, which start an

exchange reaction with metal cations. Alkali and alkaline-earth ions are leached from the structure, leaving the silica network intact. Therefore, a layer depleted in alkali and/or alkaline-earth ions is created, sometimes called hydrogen layer or gel layer. The de-alkalinisation process weakens the glass network since the hydrogen atoms are smaller than the metallic cations they replace. If calcium or potassium – as happens in potash-silica-lime glasses – are leached out, the superficial layer shows shrinkage due to the minor volume occupied by replacing atoms [7,19]. The thickness of the leached layer depends upon multiple factors, either internal (glass chemical composition firstly) or external (i.e., liquid properties and time of exposure) [26].

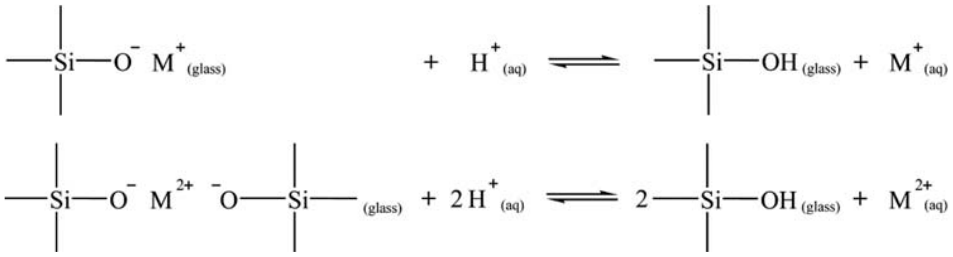

Figure 4. Stage 1 of glass corrosion. H^+ ions start an exchange reaction with metal cations and the latter are leached from the structure [19].

The stage 2 starts when the depleted layer is so thick that ion diffusion is decelerated. Due to the involvement of H^+ in the first stage, the pH at the interface between surface and solution tends to increase. The subsequent attack involves hydroxyl groups, which move towards -Si-O-Si- bonds and creates new silanol terminations (-Si-OH). Therefore, the silica network is destroyed and the dissolution of glass occurs (Figure 5) [19].

Figure 5. Stage 2 of glass corrosion. OH^- ions attack the brigdes between silicon atoms, forming silanol groups and destroying the silica network [19].

This second mechanism occurs in static contexts, where the leached layer is not removed mechanically by external agents – which would lead to the protraction of the first reaction – and where water is not renewed, but it holds the leached cations and increases the pH [7]. It seems that, while the first stage depends on ion diffusion, the second is time-dependant in a linear way [19].

The two mechanisms are competitive rather than consequent. Liquid attack begins the deterioration of the surface and if the leaching rate of the alkali cations is faster than the network dissolution one, a layer of leached-out species is created on the glass surface. On the other hand, if the dissolution of glassy matrix is faster, the structure of the glass will break and dissolve [7].

During corrosion processes, different types of glass surfaces may be formed as a result of particular interaction stages between the material and the environment (Figure 6). They are classified as follows:

- Type I surface results after the exposure to neutral solutions. The surface shows a hydrated layer less than 5 nm thick with no significant differences with the bulk composition.
- Type II surface emerges where alkali and alkaline-earth ions are leached, and a silica-rich layer is left. The glass is resistant to pH values up to 9, then the alkalinity of the medium begins the process of silica dissolution.
- Type IIIA and type IIIB surfaces have a double corrosion layer, made of an aluminium silicate or calcium phosphate film above the silica-rich layer. These films act as protection against both acidic and basic media.
- Type IV surface shows the formation of a silica-rich layer, but the content of silicon is originally so low, or the environment has a high concentration of OH^-, that the network dissolves.
- Type V surface is produced in environmental contexts with 9 or higher pH value, to which vitreous silica is soluble. Congruent dissolution occurs and corrosion pits are formed locally. Glass surface is similar in composition to the bulk [15,19,38,42].

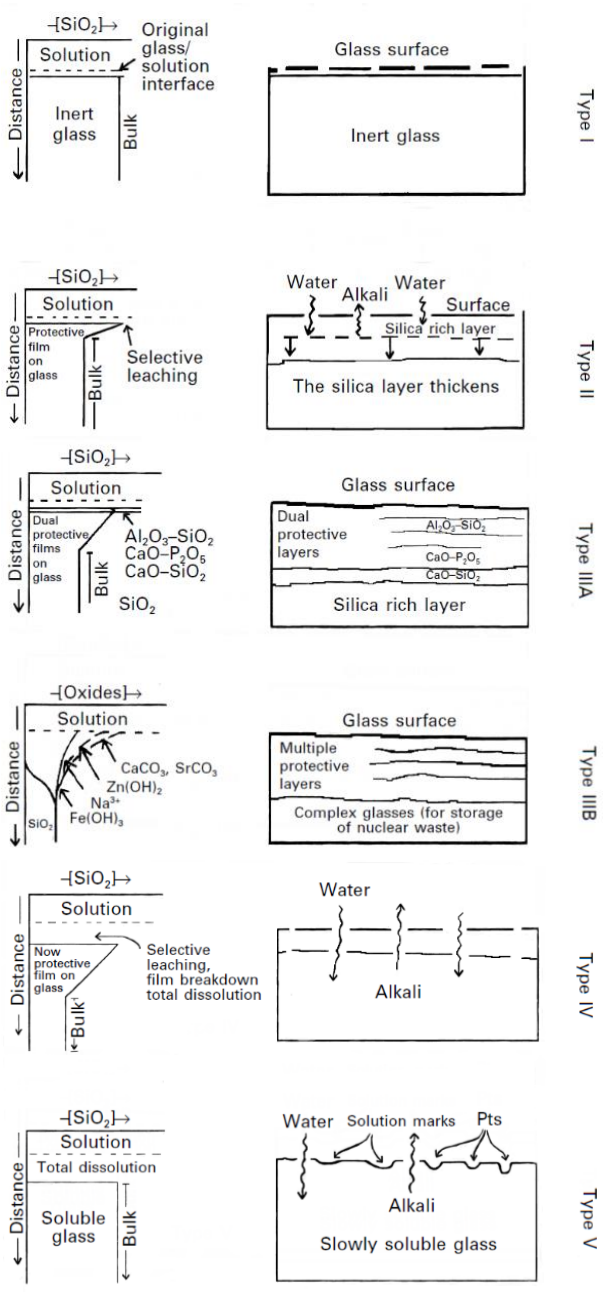

Figure 6. Types of glass surfaces formed after the interaction of the material with the environment. Modified from [7].

Among these, types II, IV and V represent the most common corrosion patterns found in archaeological glasses [42].

1.1.4.2. OTHER DETERIORATION FORMS

In the field of cultural heritage conservation we generally refer to three categories of degradation phenomena, caused by chemical, physical/mechanical and biological damage. The former includes the mechanisms described above. These are not the only phenomena acting on glasses, but certainly they are the most important ones regarding archaeological vitreous findings. Physical damages arise when the material is subject to stresses and strains greater than it can carry, bringing the artifact to break in smaller fragments. In addition, biological factors can affect glass stability through a process known as biodeterioration. Microorganisms can attack glass fragments in burial environment. They play a role in the worsening of vitreous alteration, being additional to physical, chemical, and mechanical damages [41].

1.2. SOIL

The burial environment is a complex system. In order to comprehend the mechanism leading to glass decay, we must dwell on the chemical and physical properties of soil. The present chapter aims to give the fundamental information to understand the context where the glass fragments were aged for centuries.

Soil is the portion of ground, about a couple of meters deep below the surface, which total volume is 50% made of inorganic minerals and organic matter, and air and water occupying the voids for the other half. Its composition depends on the types of rocks that were weathered and on the biochemical transformations [3,16].

The formation of soil starts with the weathering of a parent rock by atmospheric agents. With time, the processed material is deposited and horizontal layers can be noticed in the soil profile, as shown in Figure 7 [16]. The layers are called horizons and they are identified according to their physical, chemical and biological features [11]. Soil horizons are strictly related to the formation processes and the environmental context. Therefore, they are different for each soil category and climatic zone [16]. The term soil, also used in the Latin version *solum*, refers to the portion of land profile above the parent material; its upper part involved in tillage activities is called surface soil or topsoil and it is commonly characterised by a considerable amount of organic matter [3,16].

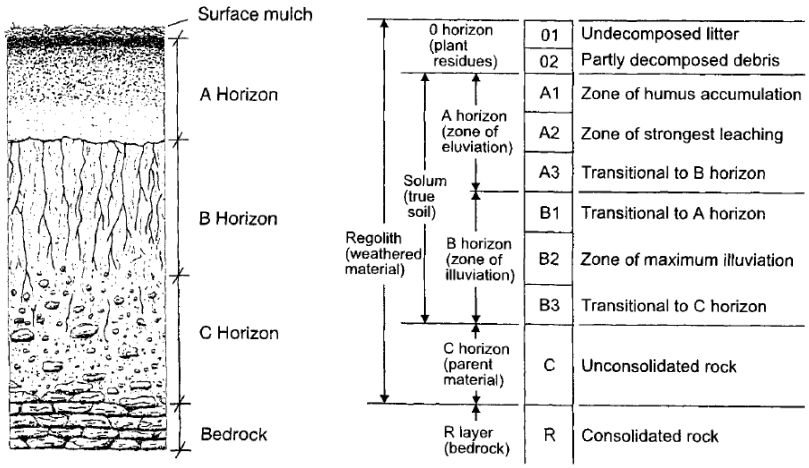

Figure 7. Soil profile (left) and characteristics of soil horizons (right) [16].

1.2.1. THE SOIL SYSTEM

As mentioned above, soil is a system including solid particles in addition to water and air occupying spaces between them, hence soil can be defined as a three-phases system (Figure 8). The solid phase is made of soil particles and it constitutes the soil matrix. The particles, different in chemical composition and shape, are both inorganic and organic, the latter usually forming aggregates with minerals. The geometric form of the soil structure describes the voids and the pores where water and air flow and are retained [11,16]. The liquid phase is the so-called soil

solution as it is the water present in the soil containing dissolved substances; the gaseous phase is the air in the voids, the soil atmosphere [16].

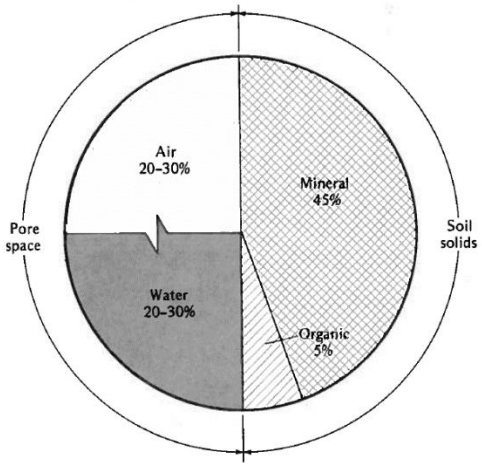

Figure 8. Representation of soil as a three-phases system [16].

1.2.1.1. THE SOLID PHASE

The soil matrix is the most important content of soil. Its mineral composition and particle size characterise the behaviour and the physico-mechanical properties of soil. The soil texture is the objective description that classifies the solid particles according to their size range. There is not a unique standard classification of the particle sizes, but all the used methods agree in the definition of soil material, which is conventionally identified as the particles having a diameter smaller than 2 mm. According to the size range, soil matter is divided into different textural fractions, namely clay, silt and sand. Each classification scheme has its own size range, and some fractions are further differentiated into subfractions (Figure 9). The material with a particle diameter greater than 2 mm is called gravel; larger fragments present in soil are classified as stones, cobbles and boulders. Sand is the fraction of soil characterised by a specific diameter ranging from 2 mm to 50 µm or 20 µm if USDA (United States Department of Agriculture) or ISSS (International Soil Science Society) classification is used. From a mineralogical point of view, it is mainly composed of quartz, but also feldspar, mica and other minerals can be found. The grains are generally associated to spheres, even though their surface is irregular and uneven [11,16]. Sand has a low water retention, but fluids and gasses are transported rapidly due to the large voids between the particles [3].

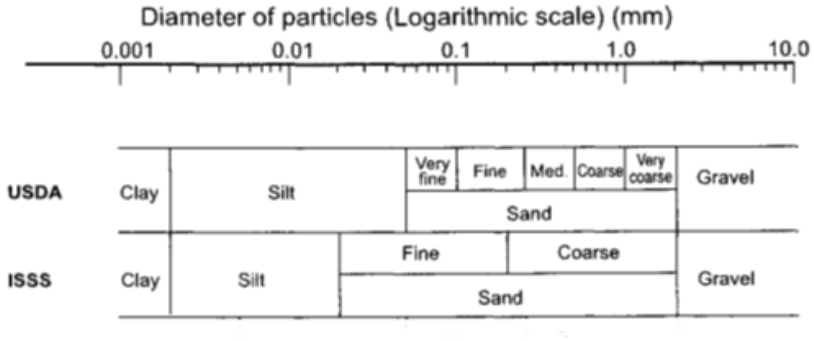

Figure 9. Classification of textural fractions of soil. Comparison between USDA and ISSS definitions. Modified from [16].

Silt is composed of particles similar to sand, but smaller in diameter. Just as sand, it consists of not weathered primary minerals coming from the parent rocks. The grains are often covered with clay, which confers clay-like properties. With a size smaller than 2 µm we have clay, plate-shaped particles. Clay is composed of aluminosilicates, that are secondary minerals formed in the transformation processes of the parent rocks, and other substances, such as oxides and carbonates. These particles are the colloidal fraction of the soil and retain water [3,11,16]. Since they have the highest surface area per unit mass, they have a great influence in the physical-chemical properties of soil, while sand and silt are relatively inert and part of the so-called soil skeleton [11,16,24]. Soils with different mass ratios between the three fractions are associated to specific textural classes [11,16].

The minerals present in soil are the result of parent rocks alteration and weathering. Primary minerals come directly from rocks, indeed they have not been chemically altered, and are silicate minerals [11,24]. According to the structural arrangement of silica tetrahedra (SiO_4^{4-}) we can identify quartz, feldspars and feldspathoids (made of a continuous network of silica), olivine (independent tetrahedra), pyroxenes and amphiboles (single or double chains of silica), micas (continuous sheets of silica). These minerals, beyond silicon and oxygen, contain metallic elements, such as magnesium, potassium, iron and aluminium [24].

Without going deeply in the spatial arrangement and specific composition of primary minerals, the focus will be on the secondary minerals that can be found in soils of temperate regions. Secondary minerals are formed by decomposition of primary ones and recombination of atoms into sheets of aluminosilicates [11,16,24], and they confer on clay the chemical and physical properties that make this fraction the principal source of soil activity [16]. Clay minerals are laminated microcrystals composed of two main structures, sheets of silica tetrahedra forming a hexagonal network by oxygens sharing, and sheets of aluminium or magnesium octahedra joined by their edges, as reported in Figure 10 [3,16,24].

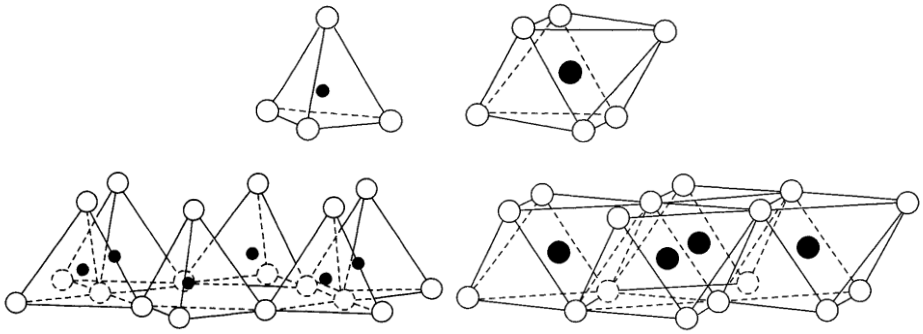

Figure 10. Sheet of silica tetrahedra (bottom left) and sheet of aluminium or magnesium octahedra (bottom right). On top the structures of a silica tetrahedron and aluminium/magnesium octahedron [16].

The main types of layered aluminosilicate minerals can be described in relation to the ratio between tetrahedra and octahedra structures, that are found stacked forming *lamellae*. In 1:1 mineral each silica sheet is linked to an octahedral sheet, whereas in 2:1 mineral one octahedral structure is in the middle of two silica tetrahedra sheets. Examples of those minerals are kaolinite and montmorillonite, respectively [3,16,24]. In world regions where the rocks were subjected to intense weathering a great part of the minerals are oxides and hydroxides of iron and aluminium mainly [3,24]. Not all minerals have a crystalline structure as those ones just described, instead some of them may show an amorphous composition. For example, allophanes belong to this category: they are made of silica and alumina components poorly structured, with various mole ratio between them and presence of phosphorus and iron oxides. They have similar behaviour of crystalline clay [16,24].

The most important feature of the clay particle is linked to the presence of various cations that are not part of the lattice structure, but they are adsorbed to its surface because of the clay negative charge. Practically, tetrahedral and octahedral structures may be subjected to isomorphous replacements, hence some principal elements of the lattice are substituted with other ions with similar radius. The net charge in the lattice changes, therefore the clay particles gain a negative charge that is balanced by adsorption of positive ions, such as sodium, potassium, or calcium among others. Since those cations are not part of the internal structure, clay can exchange them in what is called *cation exchange process* [3,16].

Part of the solid fraction in soil is constituted by organic matter. With this term we include organic debris and humus, that are the resulting transformation of flora and fauna residues [24]. Humus is responsible of the activity of organic matter as it plays a role in water retention and cation exchange properties [3,24].

1.2.1.2. THE LIQUID AND THE GASEOUS PHASES

Half of the total composition of soil is composed of water and air filling the voids between the solid particles. Water is always present in soil either in the form of free water, as that one coming from rainfalls and flowing through the soil, or as moisture present in thin layers covering the particles and adsorbed to them [11]. Water moves and it is retained by soils differently according to the physical and chemical properties of both parts. Water provides the soil solution, in which some salts are dissolved, that confers to soil a peculiar activity [3,11] as a consequence of the dynamic exchange of elements between solid particles and soil solution [3].

Air completes the soil composition. Soil air is different from the atmosphere in some features, since it has a greater level of moisture and a higher carbon dioxide content. Gasses are exchanged with soil and external atmosphere [3]. Without going in details, the most important information for the research is that water and air are included in the soil system, therefore they confer on soil specific properties that may affect the alteration on archaeological objects.

1.2.2. SOIL PROPERTIES

The composition of the three-phases system gives to the soil some specific physical properties. Examples are the texture or the porosity, that determines the movement of water and air. Besides those features, one interesting physical property of soil is its colour. The soil colour depends on the mineral and organic matter content, and it is determined and expressed accurately in terms of hue, value and chroma by matching soil samples to standardised colours in the *Munsell Soil-Color Book* [11].

Another relevant property of the soil is the electrical conductivity. Soil contains soluble salts, which presence is determined by electrical conductivity measurement. The soluble salts are either cations (Ca^{2+}, Mg^{2+}, K^{+}, Na^{+}) or anions (Cl^{-}, HCO_3^{-}, CO_3^{2-}, SO_4^{2-}) present in crystallised form or dissolved in soil solution. Those salts are different from the ions involved in ion exchange processes. The electrical conductivity of soils is proportional to the quantity of soluble salts [34].

The variable that more than all has a central role in controlling soil reactions is pH [24]. Soil acidity or alkalinity is due to the ions and compounds dissolved in the soil solution. An excess of H^{+} ions over OH^{-} anions determines the acidic character of soil [3]. Actually, the acidic pH is also determined by the presence of Al^{3+}. Aluminium indirectly contributes to soil acidity due to its hydrolysis reactions shown as Equation 1, which releases three H^{+} [3,24].

Equation 1.

$$Al^{3+} + H_2O \rightleftarrows Al(OH)^{2+} + H^{+}$$

$$Al(OH)^{2+} + H_2O \rightleftarrows Al(OH)_2^{+} + H^{+}$$

$$Al(OH)_2^{+} + H_2O \rightleftarrows Al(OH)_3(s) \downarrow + H^{+}$$

As previously explained, the soil solution is a dynamic system, therefore the pH level we may detect in soil is not only localised, but also it might change. Plant roots respiration, mineralisation of organic matter and rainfalls, which pH is 5.6 in normal conditions, are three factors contributing to continuous addiction of H^{+} ions in soil [11]. Soils have two main sources of acidity: the active acidity refers to free H^{+} and Al^{3+} ions dissolved in the soil solution, whereas the exchangeable acidity is about the ions adsorbed to soil colloids. The latter is sometimes referred to reserve acidity since those ions move into the soil solution as the pH increases. There's a dynamic equilibrium between the two sources and the soil; the soil capacity to balance pH changes by ion transfer is called *buffering* [3,24].

1.2.2.1. ION EXCHANGE

In order to comprehend the ion exchange process, we have to remember the structure of the clay minerals. As previously described, the elements in aluminosilicate minerals may be replaced by other ions. By this assumption, clay particles acquire a superficial negative charge that is balanced with the adsorption of cations, forming an electrostatic double layer. The cations can be exchanged with other positive ions in the soil solution in a rapid and reversible process called cation exchange (Equation 2) [3,16].

Equation 2.

$$Na_2[clay] + Ca^{2+} \rightleftarrows Ca[clay] + 2Na^{+}$$

A similar mechanism occurs with anions adsorbed from soil particles where the surface is positively charged and negative ions are attracted. Together, cationic and anionic exchange contribute to the ion exchange capacity, although the former mechanism is predominant [11,25]. Besides clay minerals, other sources of ion exchange are humus, amorphous minerals, oxides, and hydroxides in colloidal size; the manifestation of cation or anion exchange is referred to type of clay, organic matter, and soil pH [25].

Cation exchange capacity (CEC) is defined as the sum of positive charges of all cations that the soil can adsorb at a specific pH level per unit weight and it is expressed in milliequivalents per 100 g of soil (meq·100 g^{-1}) or in centimoles of positive charges per kilogram (cmol(+)·kg^{-1}) [11]. The phenomenon is a crucial variable in soil characterisation, as it affects the retention and the movement of ions [16].

Adsorbed cations vary in kind and quantity according to the ion concentration in soil solution and to its energy of adsorption. When these two parameters are high, the chances for adsorption increase. The adsorption energy, which may be defined as how strongly the ion is attracted by the surface, depends on the ion valence and the degree of hydration. For example, between calcium and sodium ions, the former is adsorbed more strongly than the latter, as divalent ion Ca^{2+} has twice the adsorption energy than a monovalent ion. Moreover, its hydrated radius is smaller because the size is such that the water molecules attracted by the ion positive charge are lower in amount. Na^{+} owns a greater hydrated radius because it is smaller in radius, therefore water molecules can be closer to the positive charge and higher in number, forming more layers. Due to the conditions just described, the sequence of relative adsorption energy is $Al^{3+} > H^{+} > Ca^{2+} > Mg^{2+} > K^{+} > Na^{+}$, with the former two elements indicated as acidic cations, in contrast to the other basic cations [11,25].

CEC is affected by numerous factors. One of them is the soil texture: finer textures give generally a higher CEC, but the predominance of 1:1 or 2:1 clay influences it as well. Cation exchange reactions are enhanced by the pH of the context, and they tend to be more frequent as pH increases [3].

The soil pH is tightly linked to CEC, in fact the exchangeable cations are the same contributing to the pH level and even the definition of CEC refers to pH. This means that the process is pH-dependent, even though the CEC in 2:1 clay is less sensitive to pH variations [11]. The pH of the

environment produces a temporary source of charge upon the surface of some colloidal particles. When the pH decreases, the concentration of H^+ in soil solution is high and it tends to bond with negative charges exposed on the surfaces. The result is a new positively charged surface in the particles. Otherwise, when the pH increases and the OH^- concentration is higher than H^+, the exposed charges remain negative [25].

1.3. BURIED GLASS DEGRADATION

Archaeological glass findings have been preserved in soil for thousand years before being discovered. Burial environment is a complex system where many substances interact with the material determining the modification of its physico-chemical properties. Water is the extrinsic force that, more than others, guide the occurrence of degradation phenomena. Indeed, the de-alkalinisation and network dissolution start by the presence of water. Several factors, such as the composition of the bulk glass and the manufacture details and the nature of the soil, contribute to the rise of specific visible damages [7].

The development of deterioration in burial environment results in peculiar outcomes, often similar to those produced underwater [30]. Besides the physical damages brought by direct interaction with solid particles from the soil, chemical reactions in presence of water are the main players in our context [7]. When glass corrosion is macroscopically visible, it is possible to classify surface alteration as follows:

- Dulling is the loss of glass original clarity and transparency as consequence of the changing in surface composition, which alters the refractive index. Therefore, it is different from the surface damage due to scratches, stains, or other abrasion marks.
- Iridescence is a rainbow-like effect forming on the surface after compositional changes. Generally, in multilayered structure, thickness and colour are different according to the severity of deterioration and the presence of metal oxides. The layers tend to flake away once thickened.
- Opaque weathering refers to thick laminar structure opalescent in appearance, held together and sometimes penetrated the glass bulk. When advanced alteration is present, the structure takes different colours and it is sometimes called *enamel-like weathering*.
- Cracking is the result of shrinkage due to environmental changes. In fact, the hydrated layer absorbs and desorbs water vapour and thus shrinks. This movement creates fractures that allow liquids to penetrate and continue further degradation.
- Pitting is a form of degradation occurring locally on the surface of glass and creating concentric circles and/or round pits.
- Discolouration refers to the oxidation of ions coming from the environment or present in the bulk. The effect is the creation of stains, usually dark in colour. Manganese and iron are the main responsible elements. They change the oxidation states and precipitate on the surface and between weathered layers following the reactions in Equation 3.

Equation 3.

$$Mn^{2+} + \frac{1}{2}O_2 + H_2O \rightleftarrows MnO_2 \downarrow + 2H^+$$
$$2Fe^{2+} + O_2 + H_2O \rightleftarrows Fe_2O_3 \downarrow + 2H^+$$

- The total loss of glassy nature is the ultimate form of degradation. Glass network is dissolved and only hydrated silica is left [7,40].

Archaeological glass findings show many of those degradation marks at the same time. The severity of deterioration may differ in areas of the same object, and it is function of the aggressivity of the burial context [7,40].

1.3.1. SOIL-GLASS INTERACTIONS

Buried glass degradation is the result of several factors linked to the chemical composition of glass and to the conditions of the environment.

Regarding soil, some properties are crucial in the preservation of archaeological glasses. All the aspects favouring the preservation of stratigraphic evidence, including the absence of erosion mechanisms, contribute to the maintenance of unaltered glass. In addition, soil stiffness can preserve glass from fracture. Hydrological factors have the greatest impact on buried glass artifacts, as water is the principal deteriorating agent, able to start alkali leaching, change the local pH and cause of spontaneous crack propagation [17,20]. The types and the concentration of the solutes, as well as the organic matter dissolved in soil solution, determine secondary reactions and the precipitation of specific compounds on the glass surface. The alkaline or acidic aspect of the burial context is another factor influencing the material preservation [20]. The consequences of the pH of the medium are substantial, as most of the corrosion reactions involve H^+ and OH^- species, thus affecting the preferential leaching of some cations [17].

The durability of archaeological glasses is the result of all its compositional and manufacturing features. Silica, as network former, is the most important element and its content should not be below 66% molar ratio, in order to have a proper ratio with modifiers resulting in a stable structure. In addition, calcium oxide up to around 10% molar ratio gives further stability to the glass by reducing cation extraction. This advantage is lost when lime is below 5% or above 15% molar ratio [17]. The alumina content significantly contributes to the preservation of buried glasses [12]. Moreover, the glass is more durable when alkali cations are smaller in size, since this characteristic causes them to be held strongly by the matrix. All those features are present inside Roman glasses, which show a slower corrosion than Medieval glasses on equal exposure conditions [17,19].

The methods of glassmaking and the resulting superficial features are of primary importance in the interaction with soil. A rough surface is characterised by higher surface area in contact with the weathering agents, thus favouring the deterioration processes [17].

2. MATERIALS AND METHODS

This study was carried out on some archaeological glasses obtained from the site of Aquileia (North of Italy) and on soil samples collected nearby. This section describes the materials of the study and the methods followed for the analyses. This thesis project is part of a wider research programme started at the *Center for Cultural Heritage Technology* of the Italian Institute of Technology (IIT). The experimental part was performed in collaboration with IIT researchers.

2.1. MATERIALS

2.1.1. GLASS

Sampling zones are located near Aquileia (North-East of Italy, Figure 11) and consist of some lands now exploited for agricultural purposes. This information is fundamental for the description of the context as it explains the origin of the glass fragments. The periodical ploughing of the lands led the archaeological objects to emerge. Emerged glass fragments were collected between 2011 and 2017.

Figure 11. Position of Aquileia.

Among the great number of findings, some glass fragments were selected according to the presence of alteration patina and degradation products. The glass samples studied in this research are presented in Figure 12 and a brief description is reported in Table 2. For simplicity the samples will be named with the number identifying the land where they were found. Sample 50 is L-shaped and it is the greatest in dimensions among the fragments (30x25x6 mm). It is likely to be the part of the base and the side wall of a small sized vessel which use is still unknown. Both the external and the internal surfaces are entirely covered by an iridescent multilayer with shades of blue and ochre in some parts. The surface appears very fragile and it flakes away easily. Sample 115 is a fragment intense green in colour. Its shape does not allow to hypothesise the original glass object. Pitting is visible on the surface. A great part of it is also covered by an iridescent layer. Sample 117 is a decoloured fragment small in dimensions as the previous and its surface is marked by a diffuse pitting where some dark spots are visible.

Figure 12. The glass samples selected for this case study. From left to right: sample 50, sample 115 and sample 117.

Table 2. Description of glass fragments.

Sample name	*Original land*	*Sample description*	*Inventory no.*	*Courtesy of*
50	AQ50	Biggest in size, L-shaped, likely part of a vessel, entirely covered by a fragile iridescent multilayer.	581681	*Museo Archeologico Nazionale,* Aquileia
115	AQ115	Small fragment, intense green, pitting, iridescent layer in some parts of the surface.	205239-2.2360	*Soprintendenza Archeologia, Belle Arti e Paesaggio,* Friuli Venezia Giulia
117	AQ117	Small fragment, decoloured glass, diffuse pitting, dark spots on one side.	591554	*Museo Archeologico Nazionale*, Aquileia

Glass fragments were softly washed with tap water. Particular care was taken of samples with evident superficial degradation layers. Each glass sample was collected singularly inside zipper plastic bags at environmental temperature.

2.1.2. SOIL

Soil samples were taken in July 2021 in three different lands where the glass fragments were found. Figure 13 highlights the lands of sampling. The lands are identified with the initials *AQ* followed by a number that indicates the specific land. Each of them was sampled three times with soil cores (Ø 10 cm) at different depths, namely at 30 cm, 60 cm and 90 cm in depth having the starting point at 10 cm below the footstep level. The three samples from the same land are identified by a roman number. The soil samples were collected inside zipper plastic bags and held at 4° C.

Figure 13. Map of the sampled lands near Aquileia.

The soil samples were prepared for the analysis as follows [27]: (a) The samples were roughly fractionated into small parts. (b) All the solid pieces and little rock fragments found inside the ground were collected aside. The soils were placed inside a heater at 40° C for at least 48 hours. Dry soils are shown in Figure 14. The pictures were taken at about 30 cm of distance from the samples.

Figure 14. Dry soils.

(d) Soils were fractionated and transformed into fine sand in a mortar and passed through a 2 mm sieve (Figure 15). (e) Every soil sample was divided into eight portions with a Rotating Sample Divider (Retsch). (f) For each sample two portions were successively treated with Planetary Mill Pulverisette (Fritsch) to obtain talc-like fine dust (Figure 15). The latter sample preparation is specific for MP-AES analysis. Figure 16 reports the procedures. The samples were collected at environmental temperature inside closed plastic vessels.

Figure 15. Soil preparation phases. From left to right: dry soil inside a mortar, soil passed through 2 mm sieve, talc-like fine dust soil.

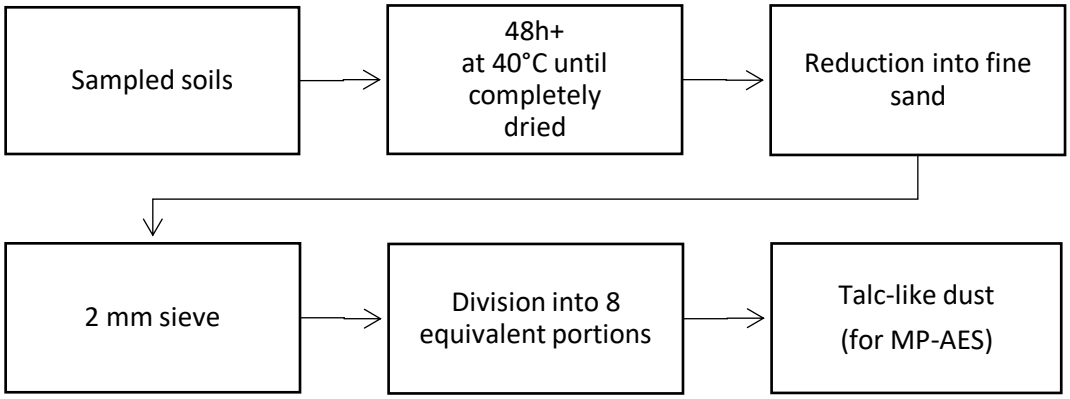

Figure 16. Scheme with the principal phases of soil preparation.

2.2. METHODS

The analyses on glass and soil samples were performed with a multi-analytical approach. The following paragraphs focus on the instrumental settings and parameters used for the analyses. For each instrument and measurement, the aim and the used method are described. A brief description about instrument functioning is presented. Quantitative analyses were performed in triplicate. All data from the instruments were collected by the dedicated software and successively elaborated with *RStudio*.

2.2.1. pH MEASUREMENTS

Acidity is one of the principal properties describing the soil and one of the main factors affecting glass preservation in burial environment [3,11,17,20,24].

The level of pH was measured on saturated solutions of the soil samples. The recommended method to assess reactivity for cultivated soils is in calcium chloride ($CaCl_2$) solution: in fact, it is not affected neither by the ratio between soil and solution nor by the concentration of soluble salts, and moreover, it results unaltered even after long air conservation of sample. Another method uses pure water as medium for the analysis [27]. Both the methodologies were performed, and the resulting values were compared consistently with the thesis aim to find best and less time consuming methods for our purposes.

The pH level was determined by potentiometric device. The analytical method from [27] requires 10 g of each soil to be added with 25 mL of $CaCl_2$ 0.01 M solution or pure water. The saline solution was prepared previously starting from $CaCl_2 \cdot 2H_2O$ solid salt dissolved in pure water and stored at room temperature. Soil and solutions were mixed in 50 mL beakers and shaken for 2 hours at 120 rpm. Samples were left to decant for some minutes and pH values were then recorded. A *benchtop meter HI5522* by Hanna Instruments was used with a *digital pH glass electrode HI10530* specific for soils. Calibration was performed with standard solutions before the measurements.

2.2.2. ELECTRICAL CONDUCTIVITY MEASUREMENTS

Electrical conductivity (EC) of soils is due to the presence of dissolved salts in soil solution. EC is a diagnostic parameter widely used to describe soil reactivity [34].

EC assessment is performed on water soil extracts in various ratios according to soil features and the desired kind of result [27]. The saturated paste extract gives more reliable indications about soil salinity. It was prepared with 10 g of soil and pure water added to moisten, left overnight and then added with water until saturated paste is formed. The extract is obtained by filtration through Büchner funnel. The extract soil-water in 1:2 ratio is used generally for soil in humid regions and intensively fertilised. It was prepared with 10 g of soil and 20 mL of pure water; samples were shaken for 2 hours at 120 rpm and decanted overnight. Then, samples

were filtered through Whatman filter paper grade 42 at least twice. Such water extracts were used for the analysis. Electrical conductivity was determined with a *conductivity electrode HI76312* coupled with *Hanna benchtop meter HI5522*. Calibration was performed with standard solutions before the measurements.

2.2.3. CATION EXCHANGE CAPACITY MEASUREMENTS

Cation exchange capacity (CEC) was assessed with the aim to determine the ion mobility in our soil samples. CEC is the sum of the cations adsorbed by soil particles; such positive ions are exchanged with the soil solution and for this reason they play a role in defining soil reactivity [3,11,16,25].

One of the most used methods to determine CEC requires the complexometric titration of the soil extracts obtained from the treatment of the samples with different solutions [27]. This methodology is time consuming as it is made of numerous work phases. In compliance with the thesis aims, a second method to determine CEC was followed, adapting the procedures described in [39] for cation analysis of water extracts. This method has been attempted because, since the cations involved in CEC are exchanged between soil particles and solution, through a simple water extraction some cations can be detected. Analysis of water soil extracts is performed to quantify available cations, but there was no indication about whether to compare the resulting value with CEC results. The detailed description of this method is reported in paragraph 2.2.6. about MP-AES analysis.

The titration method starts with 2 g of soil sample added with 25 mL of $BaCl_2$ solution at pH=8.2 inside a 50 mL centrifuge flask. The saline solution was prepared previously with $BaCl_2 \cdot 2H_2O$ salt dissolved in pure water and triethanolamine. The pH level of 8.2 was reached with the addition of HCl 1M solution. The reagent was stored at room temperature. Samples were shaken for 1 hour at 150 rpm and then centrifuged for 10 minutes at 6000 rpm. The supernatant was removed. These phases regarding the rinsing with $BaCl_2$ solution were repeated three times totally. Samples were rinsed with 30 mL of deionised water, centrifuged for 10 minutes at 6000 rpm and the supernatant was removed. To get the CEC results it is important to weight the samples, the centrifuge flask with sample before any addition, and the vessel with sample after water rinsing. Soil residues were added with 25 ml of $MgSO_4$ 5 $cmol \cdot L^{-1}$ solution. The solution was prepared previously with $MgSO_4 \cdot 7H_2O$ dissolved in pure water and stored at room temperature. Samples were shaken for 5 minutes at 150 rpm and then centrifuged for 10 minutes at 6000 rpm. The supernatant is the sample to be titrated. The scheme in Figure 17 shows the procedure just described.

The complexometric titration was carried out using ethylenediaminetetraacetic acid (EDTA) 2.5 $cmol \cdot L^{-1}$ as chelating agent. It was previously prepared from the disodium EDTA salt dissolved in pure water and stored at room temperature. A buffer solution at pH=10 was prepared with NH_4Cl and NH_4OH dissolved in pure water. The solution to be titrated was made of 10 ml of $MgSO_4$ soil solution, 100 mL of deionised water, 10 mL of buffer solution at pH=10 and the indicator made of sodium chloride and eriochrome black T. Blank solution was prepared in the same way but adding 10 mL of fresh $MgSO_4$ solution. The final volume was recorded when the solution turned blue. The CEC value of soils is derived from the EDTA amount added for titration.

The principle which the titration method relies on is the saturation of soil sample with barium and the addition of known solution of $MgSO_4$. The exchange reaction between Ba^{2+} and Mg^{2+} brings the formation of insoluble $BaSO_4$. The total content of barium added saturating the sample is exchanged with magnesium: this means that the excess of Mg^{2+} in solution, which is determined by complexometric titration with EDTA, regulates the content of barium exchanged. Lower is the concentration of Mg^{2+} in solution and higher is the CEC of the soil because it has exchanged a great part of Ba^{2+} content with Mg^{2+}.

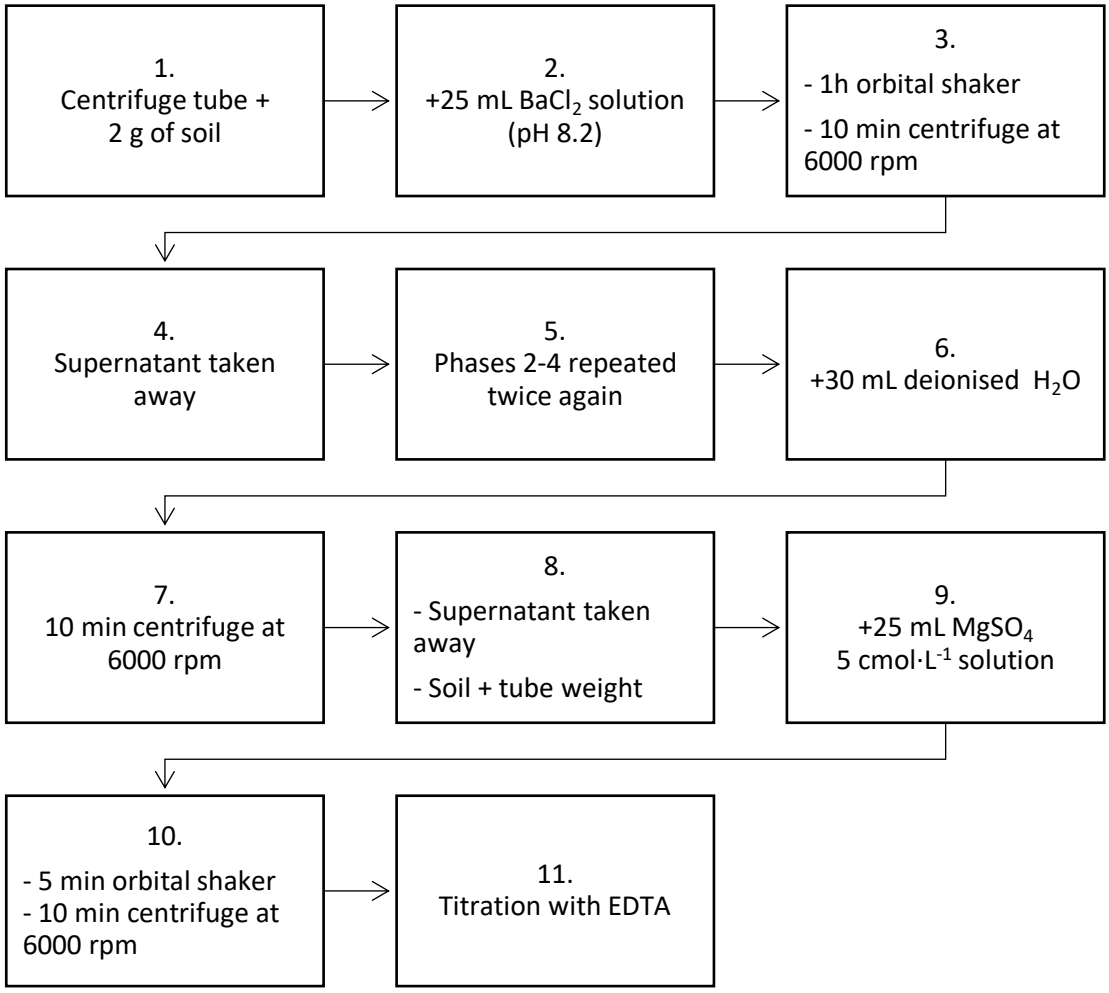

Figure 17. Scheme with the phases of CEC method.

2.2.4. OM AND SEM-EDS

The presence of alteration layers in ancient glass was investigated by Optical Microscopy (OM) and Scanning Electron Microscope Energy Dispersive Spectrometry (SEM-EDS). Preliminary observations were made with *Nikon SMZ745T Stereo Microscope* coupled with *Alexasoft TP5100 Sony CCD sensor* at 1x, 2x, 3x, 4x and 5x magnification. The visual analysis was completed with *Olympus XP43 Microscope* at x10, x20, x50 magnification. Microscopic observation of ancient glasses did not need sample preparation other than the cleaning described in paragraph 2.1.1.

Scanning Electron Microscope Energy Dispersive Spectrometry (SEM-EDS) was adopted to observe glass fragments at higher magnification and, at the same time, to study the elemental composition of the alteration patinas present on their surfaces. SEM exploits an electron beam generated by an electron gun and focused on the specimen with electromagnetic lenses. The interaction between the beam and the atoms of the surface produces several different types of signals, such as electrons or X-rays, according to the kind of interaction. The morphology of the sample is derived from the backscattered electrons detected, and EDS makes use of the emitted X-rays to identify the elements. The schematic structure of the instrument is shown in Figure 18. Samples need to be prepared before the analysis: small pieces are selected and placed on the sample plate and for nonconductive specimens a metal coating or a carbon tape is used to allow the analysis [37].

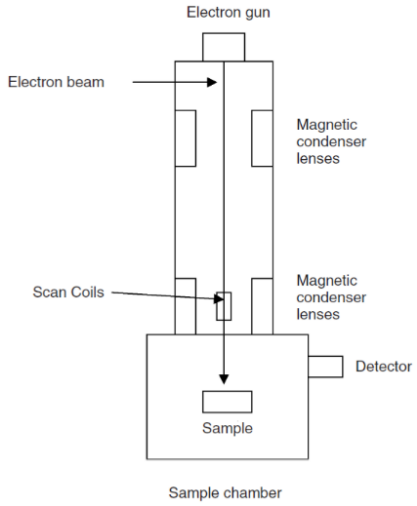

Figure 18. SEM schematic view [37].

A *Jeol JSM-6490LA Scanning Electron Microscope* equipped with a tungsten filament operating at 5 KeV accelerating voltage was used for the analysis. Small sections of the original archaeological glasses were detached and placed on the sample plate of the instrument. Carbon tape was used as glass is a nonconductive material. EDS analyses searching for Si, O, Fe, Na, Ca, Mg, K, C, S, P were performed at 15 KeV accelerating voltage. *Jeol SEM* software was used to run the analysis and collect data.

2.2.5. SPECTROPHOTOMETER

Colour is a physical feature of soil. Soil scientists define objectively the colour of soil following a three-coordinates system developed by A. Munsell. Munsell notation is made of hue, value and chroma, which are respectively the colour, the lightness grade and its saturation. Colour is assessed by matching specimen with colour charts: each chart is dedicated to one specific hue, identified with a number and a letter, and all the variations of it are ordered according to value and chroma; apertures are placed between the colour chips to compare with the sample [36]. The description of soil samples according to Munsell notation can be reached by means of spectrophotometric analysis, as in our case.

Colorimetric measurements were performed on soil samples with a *Konica Minolta Spectrophotometer CM 700d* with 10° observer and D65 as primary source of illumination. The instrument gives three numeric coordinates about colour space L*a*b* and the related reflectance spectrum. For each measure, the instrument takes SCI and SCE data, which are respectively Specular Component Included – so the specular reflection is included with the diffuse reflection – and Specular Component Excluded – in which only diffuse reflection is measured. The instrument expresses the colour sample coordinates in Munsell notation as well. Calibration of the instrument was done before the measurements. The data were collected by the instrument software *SpectraMagic NX* and elaborated in *RStudio*. Three different spots were analysed for each sample and the mean value is derived from those values.

2.2.6. MP-AES

Soil characterisation was conducted in order to understand the environmental context where glass samples were buried and preserved for centuries. To analyse the element composition soils needed to be prepared in a medium suitable for the instrument and equally able to digest totally the organic and inorganic matter.

Total digestion of soil samples was carried on with *Milestone Ethos Up microwave digestion system* following one of the operative methods included in the *easyControl* software of the instrument and specific for soil digestion. The procedure requires 0.1 g of soil added with 3 mL of aqua regia, 1.5 mL of concentrated HF and 3 mL of pure water. Aqua regia was prepared with concentrated HCl and HNO_3 in 3:1 ratio. Blank sample was prepared using the same procedure without any initial soil mass. To control the digestion grade, a sample of standard reference material 2711a Montana II soil was digested in the same conditions. The microwave run the digestion for 1 hour reaching 200° C of temperature. After 30 minutes of cooling, digested samples were added with 3 mL of H_3BO_3 oversaturated solution. Digested soil samples were left to rest for 15 minutes and then brought up to 50 mL volume with pure water inside 50 mL centrifuge flasks. Samples were stored at low temperatures.

Soil samples were analysed with *Agilent 4210 Microwave Plasma Atomic Emission Spectroscopy (MP-AES)*. This technique allows to bring the atoms of the specimen to an excited state. The quantification is performed by analysing the electromagnetic emission due to the return to the fundamental state. The liquid sample is introduced in aerosol form by a nebuliser and a spray chamber, and it is ionised in the plasma torch. Microwaves produce hot plasma of nitrogen extracted from air [1]. The instrumental parameters were as follows: pump speed was set to 15 rpm and the nebuliser flow was optimised for the current samples. Three repetitions were set for each element detection. Calibration curves were accepted with correlation coefficient greater than 0.999 and less than 10% calibration fit error was set for each standard element. To remove sample residues in the nebulisers between one measure and another, 2% HNO_3 was used as rinse solution. The wavelengths chosen for the analysis (Table 3) were selected to minimise the spectral interferences. Different calibration curves were prepared for the analysis:

- For Na, Mg, K, Al, Fe the calibration curve was configured with 0.5 ppm, 1 ppm, 5 ppm, 10 ppm and 30 ppm multielement standard solutions.
- For Zn and Sr the calibration curve was configured with 0.1 ppm, 0.5 ppm, 1 ppm and 2 ppm multielement standard solutions.

- For Cu, Ni, Co, Pb, Mn, Cd the calibration curve was configured with 0.05 ppm, 0.1 ppm, 0.5 ppm, 1 ppm, 3 ppm and 10 ppm multielement standard solutions.
- For Ca the calibration curve was configured with 0.5 ppm, 1 ppm, 5 ppm and 10 ppm standard solutions.

The standard solutions were prepared from element reference solutions in 2% HNO_3. Soil water extracts were diluted 1:10 or 1:50 to detect Ca. Other elements were detected without sample dilutions. *MP Expert* software was used to run the analysis and collect data. Data elaboration was done with *RStudio*.

Table 3. Wavelengths selected for detecting elements with MP-AES. Some wavelengths were used for the water extract for soil CEC analysis.

Element	*Wavelength (nm)*	*Type of analysis*	
		Characterisation	*CEC*
Al	396.152	✓	✓
Ba	455.403		✓
Ca	422.673	✓	✓
Cd	228.802	✓	
Co	345.351	✓	
Cu	324.754	✓	
Fe	371.993	✓	✓
K	766.491	✓	✓
Mg	285.213	✓	✓
Mn	403.076	✓	✓
Na	588.995	✓	✓
Ni	352.454	✓	
Pb	283.305	✓	
Sr	407.771	✓	
Zn	213.857	✓	

To access the total amount of elements respect to the soils, the instrumental results were adjusted with relative humidity (RH%) factors. RH% was derived from the weighting of soil samples kept at 105° C for 24 hours in muffle oven.

MP-AES was used for the alternative method to determine soil cation exchange capacity, as previously mentioned. The water extraction method requires 2.5 g of soil added with 25 mL of deionised water inside 50 mL centrifuge flasks. Samples were shaken for 30 minutes at 150 rpm and then centrifuged for 10 minutes at 6000 rpm. The solutions were filtered through Whatman filter paper grade 42 and added with 100 µL of concentrated HNO_3 to bring the pH value lower than 2. This precaution was taken to avoid iron precipitation, which could have led to other cations precipitation. Blank sample was prepared only with deionised water and concentrated HNO_3 in the same quantities. The extracts were stored at low temperatures and analysed with *Agilent 4210 MP-AES*. The instrument was set as described above; the nebuliser flow was optimised for the current samples. The wavelengths chosen for the analysis (Table 3) were selected to have as less spectral interferences as possible. The calibration curve was configured with 0.25 ppm, 0.5 ppm, 1 ppm, 5 ppm and 10 ppm multielement standard solutions containing Na, Ca, Mg, K, Ba, Al, Fe, Mn, prepared from element reference solutions in 2% HNO_3. Soil water extracts were diluted 1:5 and 1:10 to detect Mg, Ca, and Na. Other elements were detected without sample dilutions. *MP Expert* software was used to run the analysis and collect data.

Data elaboration was done with *RStudio*. The instrumental results were adjusted with relative humidity (RH%) factors. RH% was derived from the weighting of soil samples kept at 105° C for 24 hours in muffle oven.

2.2.7. LA-ICP-MS

Elemental composition analysis of archaeological glasses was implemented through Laser Ablation Inductively Coupled Plasma Mass Spectrometry (LA-ICP-MS). This instrumental setup allows to perform the analysis directly on solid samples and to map the presence of elements. Three-dimensional maps about chemical composition of samples can be created [32,33]. The schematic representation of the instrument is shown in Figure 19.

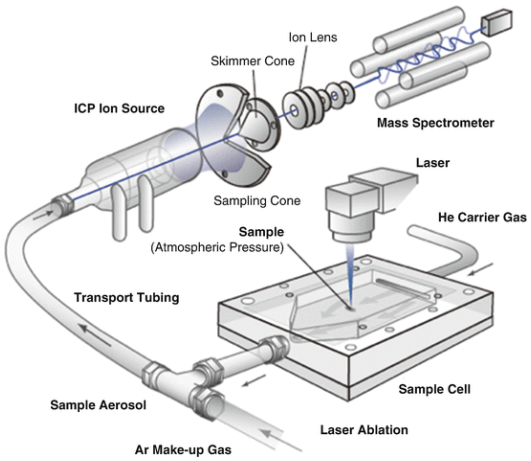

Figure 19. LA-ICP-MS schematic view.

The instrument exploits the laser ablation introducing the solid sample into the ablated cell: the laser ablates the material from the surface and the particles produced are injected into the plasma. The plasma torch vaporises and ionises the ablated material. The ions travel through the optics and they are detected by the mass spectrometer according to their mass/charge ratio [37].

The LA-ICP-MS setup employed comprises a *Thermo iCAP-RQ quadrupole ICP-MS* and a *Teledyne CETAC Photon Machines Analyte Excite ArF* excimer193 nm laser*. The laser ablation system contains a *HelEx II 2-volume ablation cell* on a high-precision xy-stage. Helium was used as a carrier gas for aerosol transport from the sample surface to the ICP-MS, with flow rates for cell and inner cup tuned to maximise transport efficiency. The *Aerosol Rapid Introduction System* (ARIS) was integrated, which is an add-on for *Teledyne CETAC Technologies laser ablation system*, capable of further enhancing the aerosol washout to the millisecond range. Before entering the plasma, the aerosol is additionally mixed with Ar as a make-up gas in the ARIS mixing bulb. The ICP-MS is equipped with quartz injector and torch, Ni cones and high sensitivity insert.

The maps were obtained using a linear scan mode with a 20x20 µm square spot size, a laser energy flux of 4 $J \cdot cm^{-2}$, and high fixed dosage. To generate 2D elemental maps, glass samples were rastered by scanning with the laser beam over the surface. Similarly, to generate 3D elemental maps the area of the glass samples was analysed in scanning mode. Six elements

were routinely recorded per image, depending on the specific glass sample composition, choosing among ^{23}Na, ^{27}Al, ^{29}Si, ^{39}K, ^{43}Ca, ^{55}Mn, ^{57}Fe, and ^{59}Co.

The ICP-MS operating parameters adopted for the analysis are reported in Table 4. All the data elaboration including background subtraction and image construction were performed using the software *HDIP (Teledyne Photon Machines*, Bozeman, MT, USA).

Table 4. Operating parameters adopted for LA-ICP-MS analysis.

Laser ablation	*Analyte Excite ArF excimer*
Wavelength	193 nm
Spot size	20 µm
Fluence	4 J·cm^{-2}
Repetition rate	280 Hz
Scanning speed	800 µm·s^{-1}
Fixed dosage	7
Penetration rate	150 nm per pulse (in glass)
ICP-MS	*iCAP-RQ quadrupole*
Isotopes measured	^{23}Na, ^{27}Al, ^{29}Si, ^{39}K, ^{43}Ca, ^{55}Mn, ^{57}Fe, ^{59}Co

3. RESULTS

3.1. GLASS ANALYSES

Archaeological glass samples found in the site of Aquileia (northern Italy) were studied with several analytical techniques to identify the nature of alteration patinas and degradation products present on the surface. The studied glass fragments are different in shape, dimension, colour, and degradation pattern. The sample 50 is the one presenting the most distinct degradation features, with both the external and the internal surfaces entirely covered by blue and ochre iridescent multilayer. The altered layer is very thick and only with microscopic observations the original glass colour can be revealed. The sample 117 is marked by a diffuse pitting and some dark spots are visible as well. The sample 115 has degradation features similar to both the other fragments. Pitting is visible on the surface and a great part of it is also covered by an iridescent layer.

The superficial extension of alteration patinas and the presence of degradation products were verified observing glass fragments under the microscope. Sample 50 is the most striking to observe, as the iridescent layer covers the entire surface and colour and thickness are variable from one area to another. A group of selected images about this sample is reported in Figure 20. The iridescent layer is intense blue in great part of the surface and changes in shade between whitish, ochre, light blue, green and pink in different zones. In some areas the multilayered structure of the patina is clearly visible. Some thick intrusions in relief are found. They are long-shaped and made of many concentric layers around an internal straight structure. In some areas the patina is narrow, fragile and discontinuous. Plenty of small flakes of patina are lost leaving the pristine glass accessible. It is possible to assess the original colour of the archaeological glass object, a dark shade of blue, close to black. Underneath iridescence, the surface of the fragment is uneven as it is signed by plenty of round pits of different sizes. Some of those pits are filled with soil.

Surface degradation of sample 115 is appreciable at naked eye. Some selected images of the sample are displayed in Figure 21. Diffused pitting covers the entire surface and the optic effect of iridescence is present in some areas. Under the microscope the pits appear roundish in shape and various in size. The iridescence patina is thinner than it is in sample 50 and its multilayered structure is not evident. In some areas the patina is not visible.

Expanded pitting characterises the surface of sample 117. Images about the sample are collected in Figure 22. Pits are similar in size and shape. They are round shaped and developed in the depth of the glass. Soil deposits are found in the inside. Few pits greater in size can be noticed. Generally they are called *rings* and they differ from pits because of the concentric circular depositions in the inside. Rings formation is still unknown. Some dark spots are visible as well. Those marks appear as dark encrustations localised on some points of the glass surface. Microscopic observations lead to notice the presence of an ultra-thin layer of iridescence. In the areas where present, the patina is continuous, transparent but with the typical optical effect.

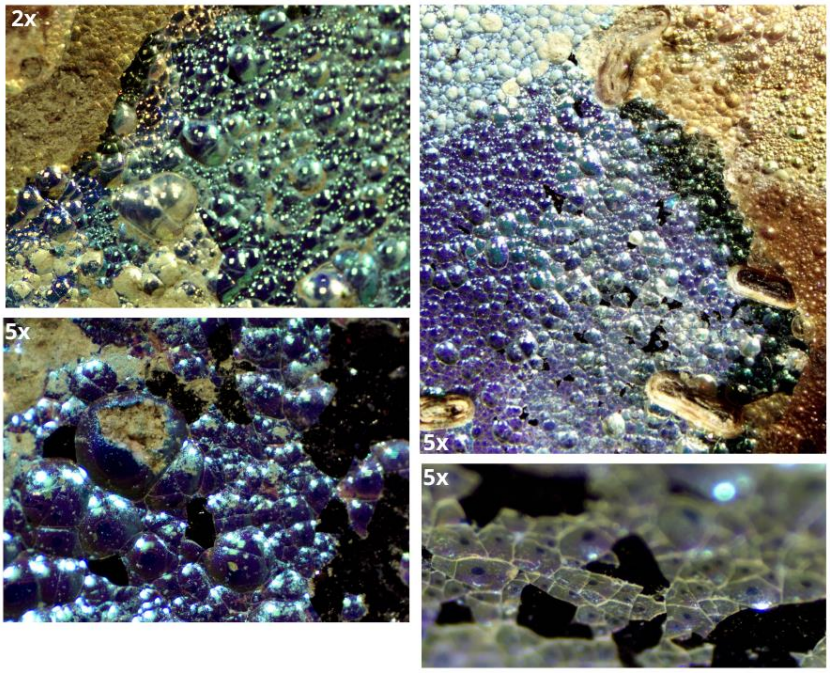

Figure 20. Pictures about sample 50 under the stereomicroscope. Magnification is reported on the images.

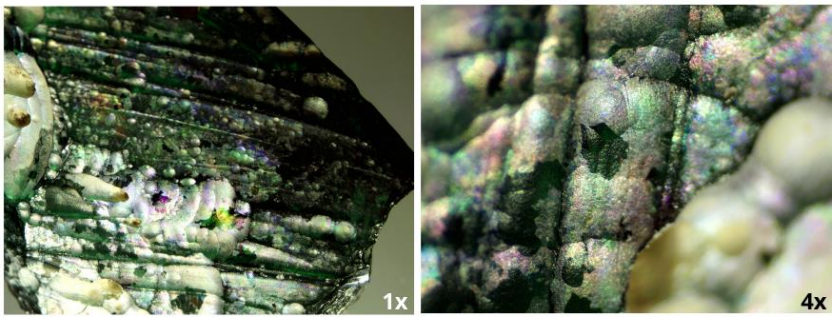

Figure 21. Pictures about sample 115 under the stereomicroscope. Magnification is reported on the images.

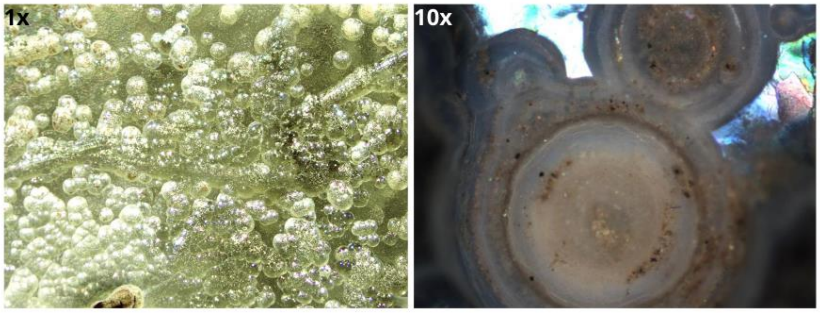

Figure 22. Pictures about sample 117 under the stereomicroscope and the OM. Magnification is reported on the images.

3.1.1. SEM-EDS

Glass fragments were analysed through SEM-EDS to study morphology and composition of alteration patinas. The thick patina developed on the surface of sample 50 was observed using secondary electrons (Figure 23). The heterogeneous structure of these corrosion products is clearly visible in the collected images. Several pits with irregular borders are observed on the surface. The outer surface of the altered patina emerges as highly fractured. In some spots the patina flaked away revealing the presence of other layers underneath. In the cross-section, at 1000x magnification the layered nature of the patina is clearly visible. The patina appeared heterogeneous both in width and in length, elements of discontinuity, probably fissures, are noticed. The thickness of the film is measured in the order of 15 µm. A flake of the iridescent patina present on the sample 50 is analysed with EDS probe (Figure 24). The image on top displays the area of analysis. Particularly, the results evidence the presence of a superficial layer enriched in Si and depleted in alkali and alkaline-earth ions, which signals are weak. The outcome of this analysis is the identification of a silica gel layer on the specimen.

Figure 25 shows the sample 115 under SEM. The visual analysis of the specimen confirms the presence of diffused pitting and alteration patina. Micro-pits can be noted on the surface. The smallest of them are isolated, perfectly round shaped, whereas the bigger ones tend to fuse together with the progression of the degradation. The EDS analysis (which is not reported here) indicates the presence of silica gel layer on the surface of the specimen, due to alkali depletion.

SEM images of the sample 117 are collected in Figure 26. The alteration patina of the sample 117 is marked by numerous little pits, with diameter equal to 500 µm or smaller. In some areas of the sample the degradation is so advanced that pits are fused together covering the entire surface. Some rings can be identified with the concentric deposits present in the inside.

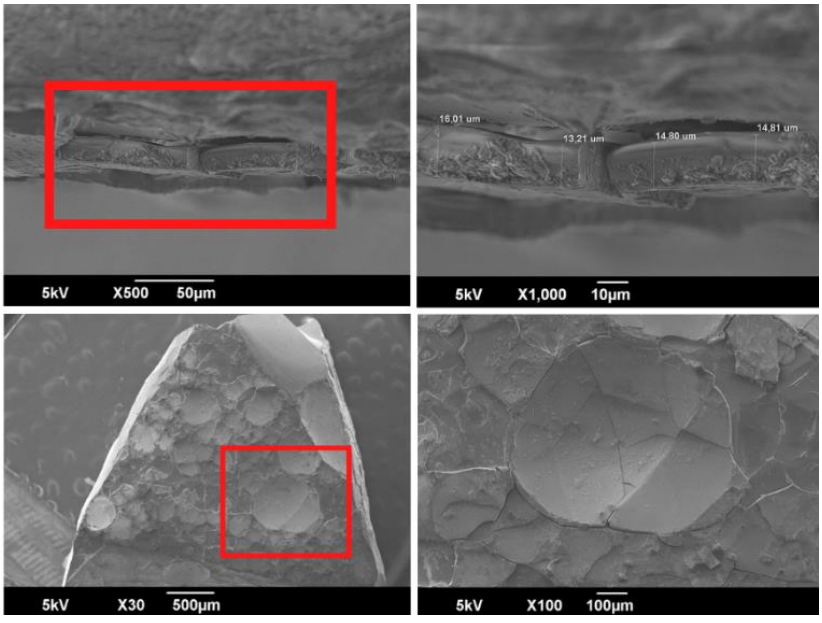

Figure 23. SEM secondary electrons images about sample 50. Accelerated voltage, magnification, and size are reported. The right images are the magnified areas highlighted on the left images.

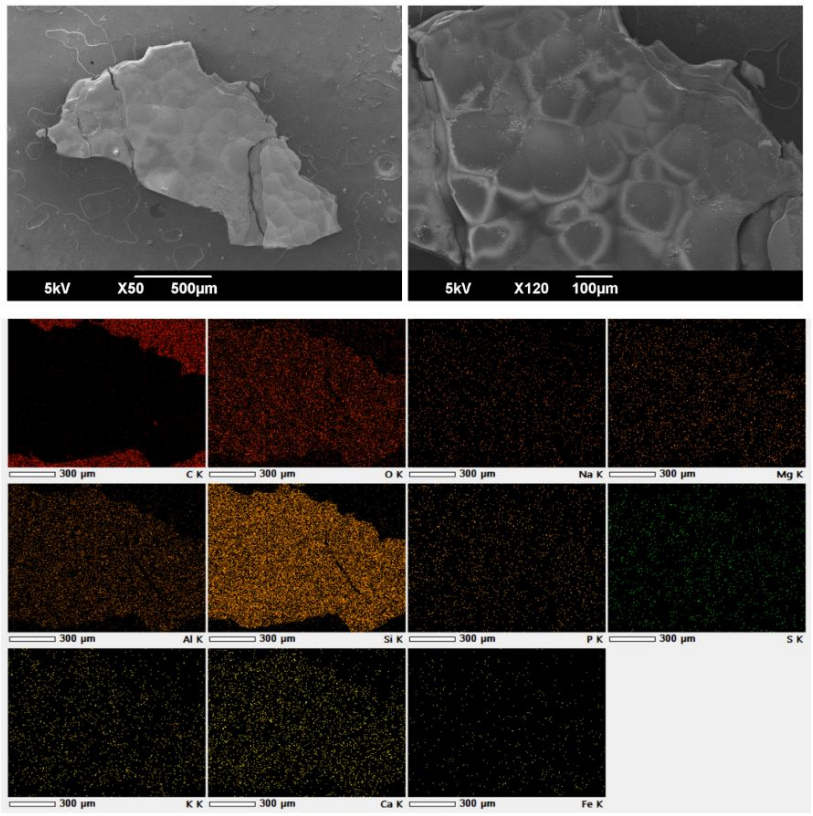

Figure 24. SEM-EDS analysis of a flake from sample 50. On top the secondary electron image of the analysed area (magnification of it on the right). Accelerated voltage, magnification, and size are reported. On bottom the results of the analysis. In the middle the elements mapped.

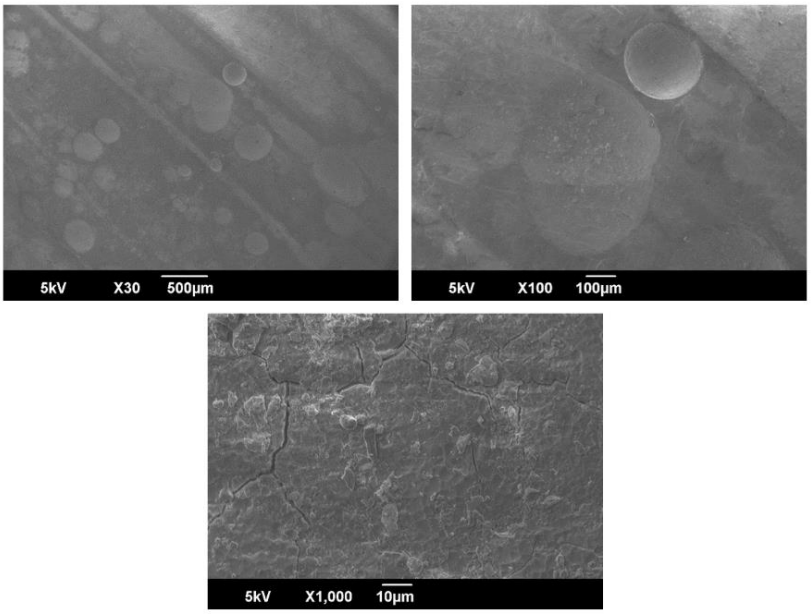

Figure 25. SEM secondary electrons images about sample 115. Accelerated voltage, magnification, and size are reported.

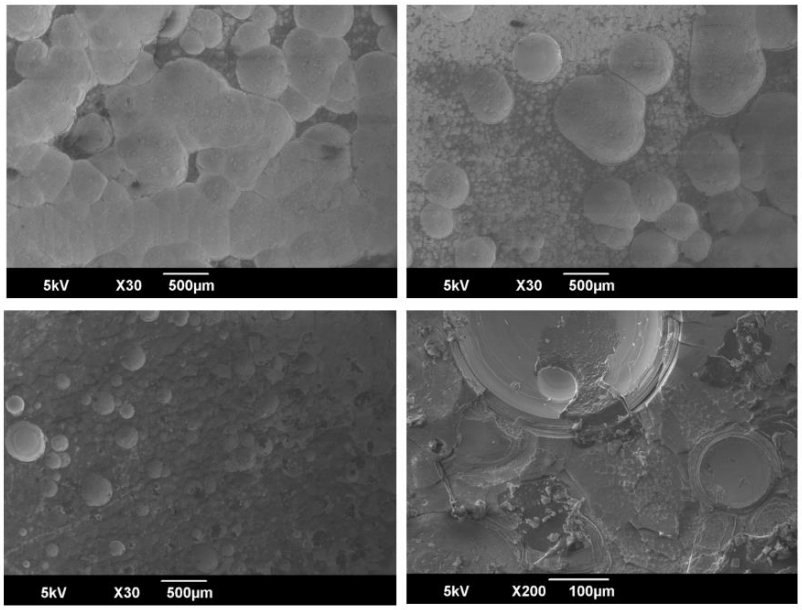

Figure 26. SEM secondary electrons images about sample 117. Accelerated voltage, magnification, and size are reported.

3.1.2. LA-ICP-MS

The analysis with LA-ICP-MS was performed by IIT researchers. Data elaboration and discussion about results were done in collaboration.

The great advantage in performing glass samples analysis with LA-ICP-MS is the creation of 2D and 3D maps. The composition of glasses can be studied at different levels as the ablation allows to access the depth of the bulk glass. Figure 27 displays an example about the potential of this instrument. The analysis regards the section of a ring structure present on the glass surface. The optical image of the ablated area is reported on top of the figure. The elemental analysis through the mass spectrometer detector identifies the presence of elements, which distribution is arranged in two-dimensional maps. Each map reports the distribution of a specific element and the lighter colour marks the areas where the intensity signal is strongest. Since the intensity is measured in counts per second this approach is qualitative rather than quantitative. Maps let to visualise additional degradation phenomena, such as micro-fissures, difficult to notice with other instruments. The maps clearly show the presence of sharp concentration gradients of leached-out ions, such as Na, Mg, K, and Ca, between the pristine glass (the area on the left of the image) and the altered surface layers (on the right in the image). The preferential distribution of Co and Mn within certain areas suggests the possible occurrence of cyclic dissolution-re-precipitation processes [22].

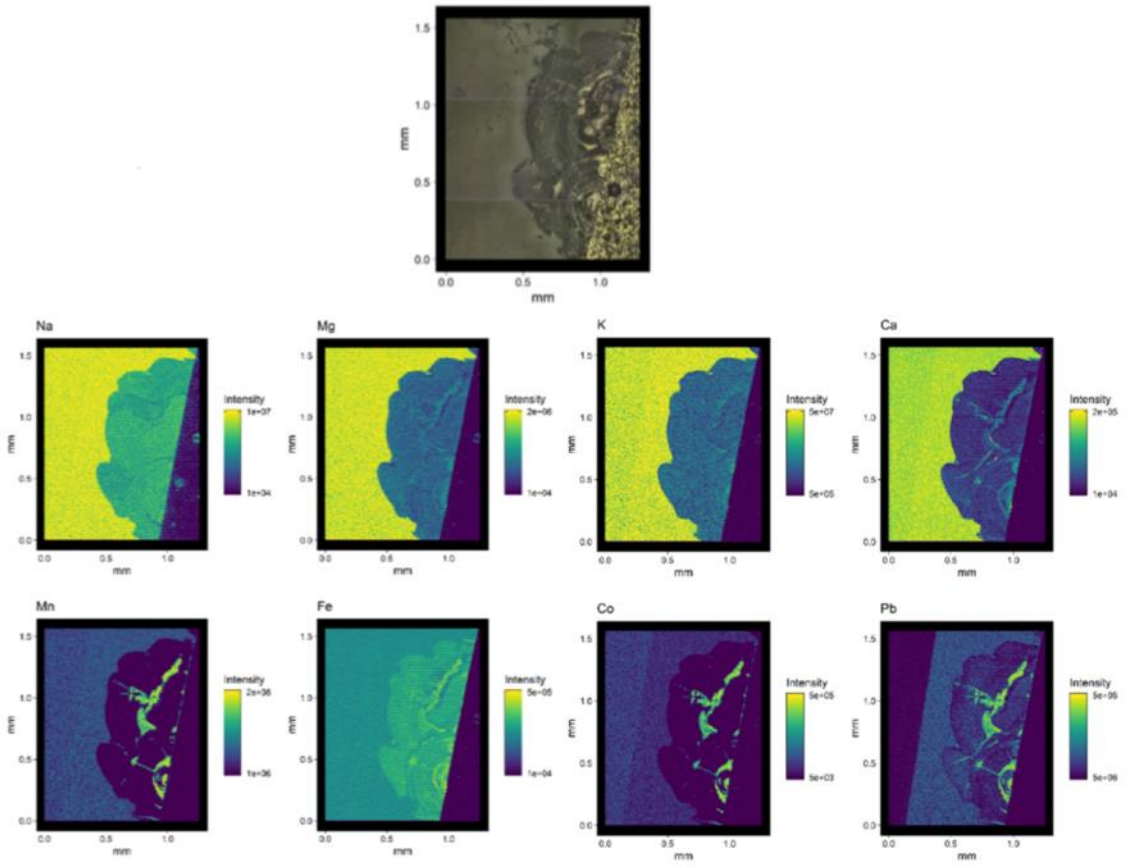

Figure 27. Example of glass analysis with LA-ICP-MS. The ablated area is a ring structure in section (on top). The two-dimensional maps display the distribution of various elements. Yellow areas have strong intensity signals. Intensity is measured in counts per second (cps).

Successive ablations of the same area of glass sample allow to study in detail the element distribution. Figure 28 shows the three-dimensional maps obtained following this method. The square spot size is of 20 µm and the depth of each ablation is between 100 and 150 nm. The image on top reports the ablated area and the successive ablations are ordered from top left to bottom right. The strong signals of the first layer of the glass surface show that the amount of the removed material was considerably higher during the first ablation. The superficial high intensities of Si and Al suggest the contamination of material from the surrounding environment where the glass was immersed for centuries. Nevertheless, the mappings indicate the decreasing of the intensity of the two elements from the surface towards the bulk of the glass, thus the enrichment of Si due to the leaching of alkali and alkaline-earth ions from the glass network. Moreover, micro-cracks emerge on the ablated surface. The cracks are not visible under the microscope even at higher magnifications. In the same way, micro-pitting is revealed as blue areas appearing in the maps about Si distribution.

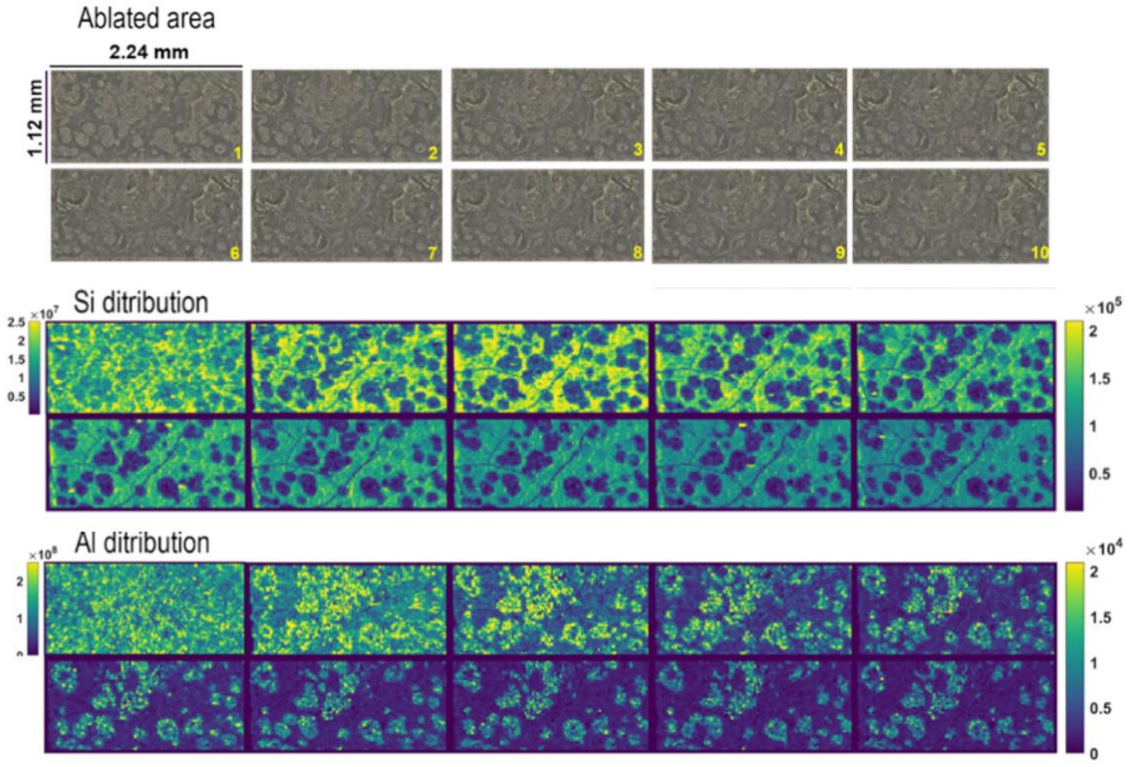

Figure 28. Example of glass analysis with LA-ICP-MS. The three-dimensional maps display Si and Al intensities signals over an area revealed by successive ablations. The first layer is on top left, the last layer is on bottom right. Yellow areas have strong intensity signals. Note that the first map has a different scale. On top the pictures of the ablated area. Intensity is measured in counts per second (cps).

The layer-by-layer elemental distribution shows how the composition changes from the surface to the bulk of the samples. In Figure 29 the profile distributions of various elements, which are collected analysing an iridescent glass sample, are shown. Each map reports the distribution of a single element: Si, Na, Mn and Co. Yellow areas point where the elements are detected at higher intensity. Note that each map has its own scale. Interestingly, in the first few nanometres of the surface the silicon signal is stronger rather than in the bulk glass. On the contrary, sodium is detected at higher intensities in the bulk of the sample, in association with Mn and Co. These metals are present in different relative contents and their distribution is heterogeneous in the depth of the patina. These maps reveal the presence of a silica gel layer and support de-alkalinisation as the main phenomenon occurring at the glass surface in burial conditions. The leaching process produces a different diffusion of the modifier ions inside the silica network, according to the nature and the atomic radius of the ion itself, an alkali cation (such as Na, with a smaller radius) or a heavy metal ion (Co or Mn, with bigger radii). The sodium depletion zone is deeper because it is smaller in radius and it has a higher mobility in the glass matrix. Instead, Co and Mn are depleted from a narrower area of the glass sample. The alteration in this sample is due to the preferential leaching process, whereby both alkali and heavy metal ions are leached out of the glass matrix but the kinetic of those elements is such to have different depths of depletion.

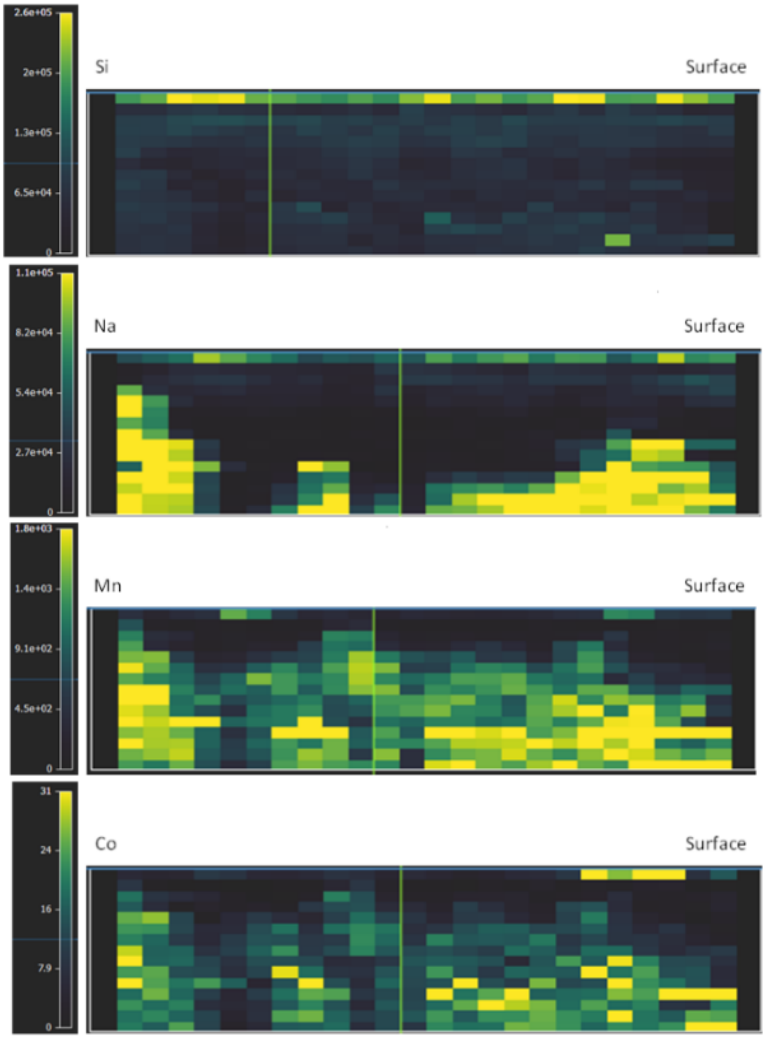

Figure 29. Example of glass analysis with LA-ICP-MS. The three-dimensional maps are about an iridescent glass fragment. Each map displays the distribution of an elements, Si, Na, Mn and Co, from the surface (top of each map) to the bulk glass (bottom). Yellow areas have strong intensity signal. Intensity is measured in counts per second (cps).

3.2. SOIL CHARACTERISATION

The environmental soils which embedded archaeological glass fragments were analysed. As previously specified in section 2.1., from each land, named AQ50, AQ115 and AQ117, three soil cores were collected at different depths. Table 5 reports a brief description of soil samples. The AQ50 land is located near the Grado Lagoon. The soil samples collected there appeared to be made of clay and were highly moistened. Few small solid pieces associated to rocks or archaeological fragments – mainly ceramics and glasses – were found. The comparison of the three oven-dried soils lead to note that the colour is darker in depth. The AQ115 and AQ117 lands are sited inland. The former was difficult to sample, because the soil core was blocked to go deeper during the third sampling. The AQ117 was sampled in a spot where the land was characterised by a light mark highly visible from satellite images and where crops grew less in height than in most of the location. Both retained a minor content of water. A great number of small archaeological fragments was found inside them. The three samplings in AQ115 are homogeneous in colour. Instead, the shades of the samples collected from the AQ117 land become lighter with depth. Following the procedures reported in chapter 2.1. soil samples were dried and disaggregated up to diameter size smaller than 2 mm before any kind of analysis. Figure 30 on the left shows the soils after preliminary preparation. Soil images are sorted from left to right by sample name and reproduce depth levels from top to bottom: 30 cm, 60 cm, and 90 cm below the surface for I, II and III level of sampling respectively.

Table 5. Description of soil samples.

Sample name	*Sampling depth*	*Description of sampled lands*	*Notes*
AQ50 I	30 cm	Near the lagoon	Clay-like soil, wet, difficult to fractionate by hand and with the mortar, few solid pieces included, going in depth it becomes darker in colour
AQ50 II	60 cm		
AQ50 III	90 cm		
AQ115 I	30 cm	Inland, difficult while sampling in depth	Less water inside, easier to fractionate, lots of solid pieces and finds included, homogeneous in colour
AQ115 II	60 cm		
AQ115 III	90 cm		
AQ117 I	30 cm	Inland, satellite images highlight a kind of light mark, crops grow less in height	Easy to fractionate, lots of solid pieces and finds included, darker, going in depth it becomes lighter in colour
AQ117 II	60 cm		
AQ117 III	90 cm		

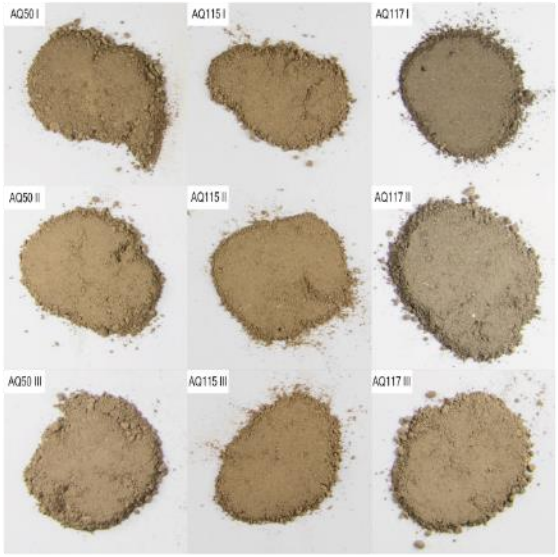

AQ50 I 1Y 6/2	**AQ115 I** 0Y 6/2	**AQ117 I** 2Y 5/1
AQ50 II 1Y 6/2	**AQ115 II** 0Y 6/3	**AQ117 II** 1Y 6/1
AQ50 III 1Y 6/1	**AQ115 III** 0Y 6/4	**AQ117 III** 2Y 6/1

Figure 30. On the left: soil samples after the preliminary preparation. On the right: description of the soil colour according to the Munsell notation system.

Figure 30 on the right reports the colour description of the soils according to the Munsell notation system. The information is arranged imitating the scheme of the image on the left. The Munsell colour notation is the most used system among soil scientists to describe the colour of the soil. Generally it is obtained through direct comparison of the soil with colour chips, but in this case a spectrophotometric measurement was used. All soils have yellow hue, with value between 5 and 6 and chroma between 1 and 3. In comparison the various shades can be noticed clearly.

3.2.1. MP-AES SOIL CHARACTERISATION

Elemental characterisation of soils was performed with MP-AES analysis. Samples were totally digested with aqua regia and hydrofluoric acid. To underline the differences between the soils a new parameter is derived, that is the mean value of data related to the three samplings. Therefore, along this discussion the values referred to the three levels of sampling will be added with the mean value, identified with the lower case letter *m* after the name of the land. All data resulted from this analysis are reported in supplementary materials (cf. ch. 7 Table S1, Figure S1). Here in Table 6 the mean values are shown. The table is about the element content expressed in $g \cdot kg^{-1}$ of soil mass. The graphical representation of data is shown in Figure 31.

Table 6. Mean values about the element content in the soil samples. Data are in $g \cdot kg^{-1}$ and the uncertainty of the measures is reported. Cd, Co and Ni are under the detection limit of the instrument. Mn, Sr, Zn contents is smaller than 1 $g \cdot kg^{-1}$.

Sample name	*Element content ($g \cdot kg^{-1}$)*							
	Al	*Ca*	*Cu*	*Fe*	*K*	*Mg*	*Na*	*Pb*
AQ50 m	35±1	10±12	<1	20±1	7.9±0.4	15±2	2.9±0.2	<1
AQ115 m	2.5±0.5	111±13	<1	<1	9±2	14±2	3.3±0.5	<1
AQ117 m	3±1	108±6	3±5	45±5	13±1	2±2	5±2	2±2

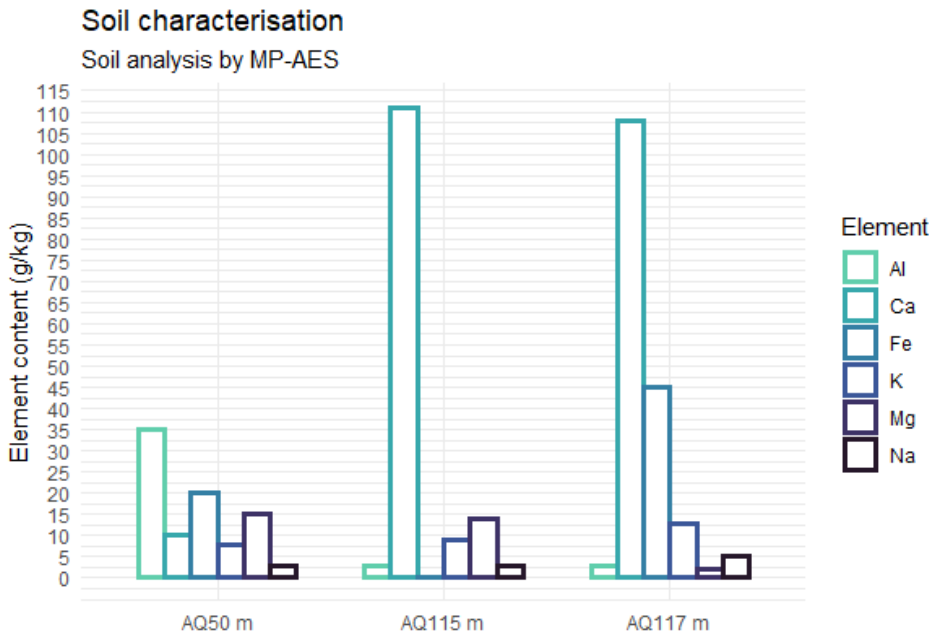

Figure 31. Graphical representation of the mean values about the main elements in the soil samples. Data are in g·kg^{-1}. Colours identify different elements.

Al, Ca, Fe, K, Mg and Na are the elements detected in higher amount in soil samples. Cu, Mn, Ni, Pb, Sr, Zn, are present at lower amounts in the order of mg·kg^{-1} of soil mass. Cd and Co content is below the detection limit. In the comparison between the soils Al, Ca, Fe, Mg and Pb amounts have the greatest variability. The quantities of Al and Ca detected in the AQ50 soil are remarkably different from the values reported for AQ115 and AQ117 (Figure 32). This difference is important to note since Al and Ca, generally present in soil in the form of silicates and carbonates, allow to distinguish a clayey soil – in this case, the AQ50 soil - from a calcareous one – the AQ115 and AQ117 soils.

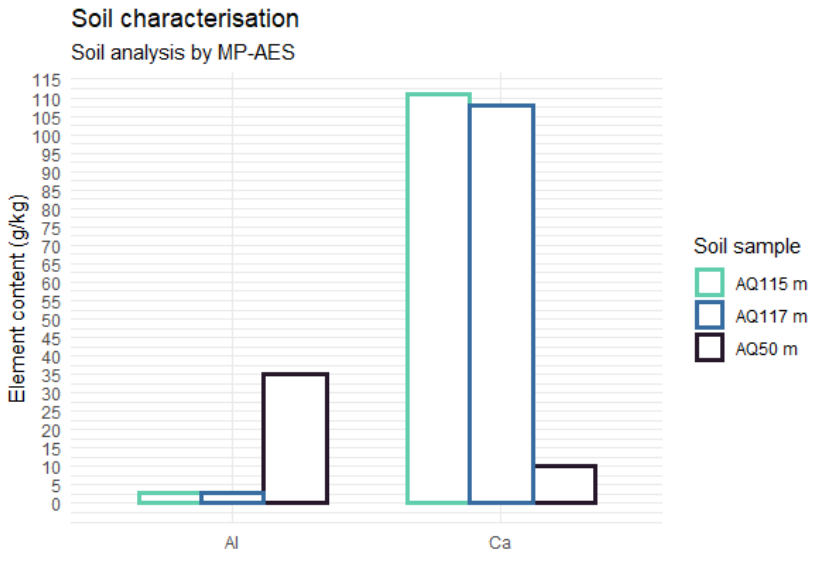

Figure 32. Graphical representation of the mean values about Al and Ca in the soil samples. Data are in g·kg^{-1}. Colours identify different soil samples.

3.2.2. SOIL pH

Table 7 reports the mean pH values of our soil samples treated with water and $CaCl_2$ 0.01 M saline solution. The latter is recommended while evaluating soil parameters since it is not affected by the concentration of the soluble salts nor by the ratio between soil and solution. Moreover, the resulting values are consistent with the H^+ actual activity in agricultural lands. The comparison with water measures wants to confirm this statement and to show the difference between the two analytic liquid media. The table clearly shows the difference between the two, for that reason we will consider the results obtained with the saline solution. The AQ115 and AQ117 soils have similar pH values, just above 8, indicating the sampled land as moderately alkaline, while AQ50 appears neutral. In supplementary data (cf. ch. 7 Table S2, Figure S2) the heterogeneities of results are noticed. The pH values of the AQ115 and AQ117 samples range between 7.9 and 8.2, confirming the alkaline nature of the soils at the three levels of sampling. In contrast, AQ50 shows a peculiarity: the first 30 cm of depth has 7.5 pH value, which identifies it as slightly alkaline, but the level decreases to 7.1 for the 60 cm in depth until the strongly acidic value of 5.4 for the deepest sample (Table 8). Also the results obtained in water medium confirm the decrease of the pH value for AQ50. Figure 33 displays data graphically.

Table 7. Mean values about pH in the soil samples. Data refer to the measures in saline solution and in aqueous solution. The uncertainty of the measures is ± 0.1 pH.

Sample name	*pH values*	
	$CaCl_2$ solution	*H_2O solution*
AQ50 m	6.7	6.8
AQ115 m	8.1	8.6
AQ117 m	8.1	8.5

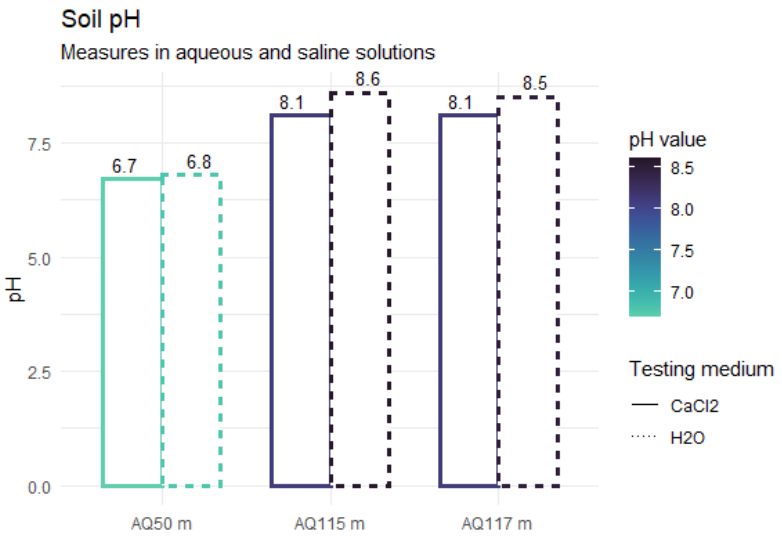

Figure 33. Graphical representation of the pH values in the soil samples. For each soil the value measured in two testing media is reported. Colour is function of pH level.

Table 8. Data about pH value in the samples from AQ50 soil. Measures from two testing media are reported. The uncertainty of the measures is ± 0.1 pH.

Sample name	*pH values*	
	$CaCl_2$ solution	*H_2O solution*
AQ50 I	7.5	7.8
AQ50 II	7.1	7.2
AQ50 III	5.4	5.4
AQ50 m	*6.7*	*6.8*

3.2.3. SOIL ELECTRIC CONDUCTIVITY

The total amount of soluble salts in soil was assessed indirectly with electrical conductivity (EC) measurement. Two methods were followed, the saturated paste and the extract soil-water in 1:2 ratio. The former was set but the extract was not such to allow the electrode measure. The results from the measure of the water extract are presented in Table 9. The values are expressed in $\mu S \cdot cm^{-1}$. For this analysis the mean value is not derived due to the high variability of data about the AQ50 soil. The latter has an EC value extremely high than the values about AQ115 and AQ117. Data related to the three levels of sampling in AQ50 reveal the increment of EC value with a peak in AQ50 III. Both AQ115 and AQ117 have homogeneous data at the different depths. Figure 34 visualises data.

Table 9. Mean values about the soil electric conductivity. Data are in $\mu S \cdot cm^{-1}$. The uncertainty of the measures is ± 0.1 $\mu S \cdot cm^{-1}$.

Sample name	*EC values ($\mu S \cdot cm^{-1}$)*
AQ50 I	442.6
AQ50 II	682.2
AQ50 III	2152.0
AQ115 I	271.9
AQ115 II	267.8
AQ115 III	252.0
AQ117 I	368.9
AQ117 II	329.8
AQ117 III	357.5

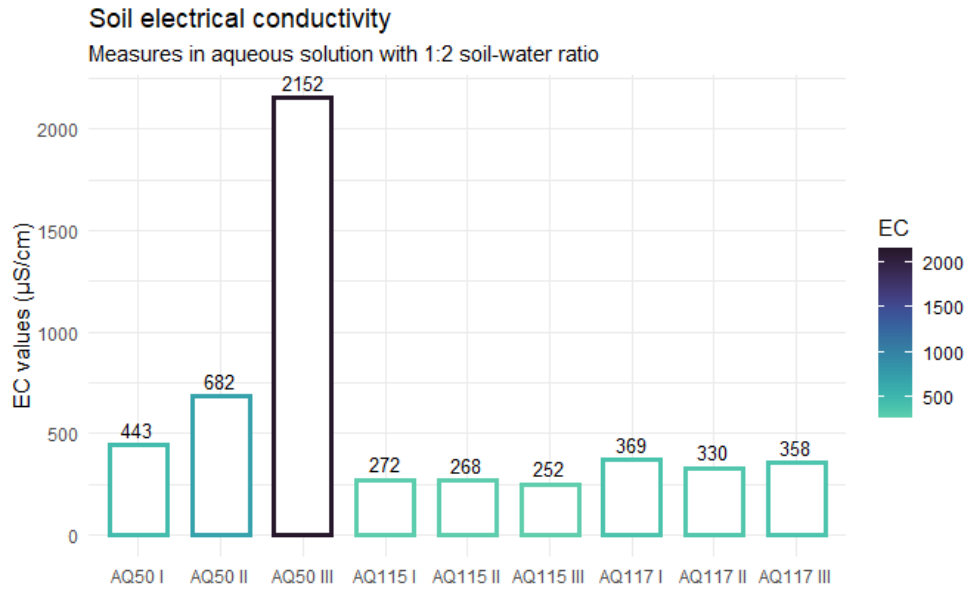

Figure 34. Graphical representation of the electrical conductivity in the soil samples. Data are in µS·cm^{-1}. Colour is function of the EC value.

3.2.4. CATION EXCHANGE CAPACITY OF SOIL

Soil characterisation was completed with the assessment of cation exchange capacity (CEC). The complexometric titration method was followed combined with a water extraction procedure to verify that the same result would be reached in a new way.

Table 10 collects the CEC values expressed in cmol(+)·kg^{-1} of soil mass. Figure 35 visualises data. Although the capacity to exchange cation is elevated in all the soil samples, AQ50 show the highest value. As it can be seen in supplementary materials (cf. ch. 7 Table S3, Figure S3), CEC values about AQ50 and AQ115 are homogeneous, whereas data about AQ117 have a different trend (Table 11). The exchange capacity decreases with depth. Note how much the value associated to the second level of sampling – that is 60 cm below the footstep level – varies from the value revealed in AQ117 I.

Table 10. Mean values about the cation exchange capacity in the soil samples. Data are in cmol(+)·kg^{-1} and the uncertainty of the measures is reported.

Sample name	*CEC values (cmol(+)·kg^{-1})*
AQ50 m	43±7
AQ115 m	24±3
AQ117 m	29±17

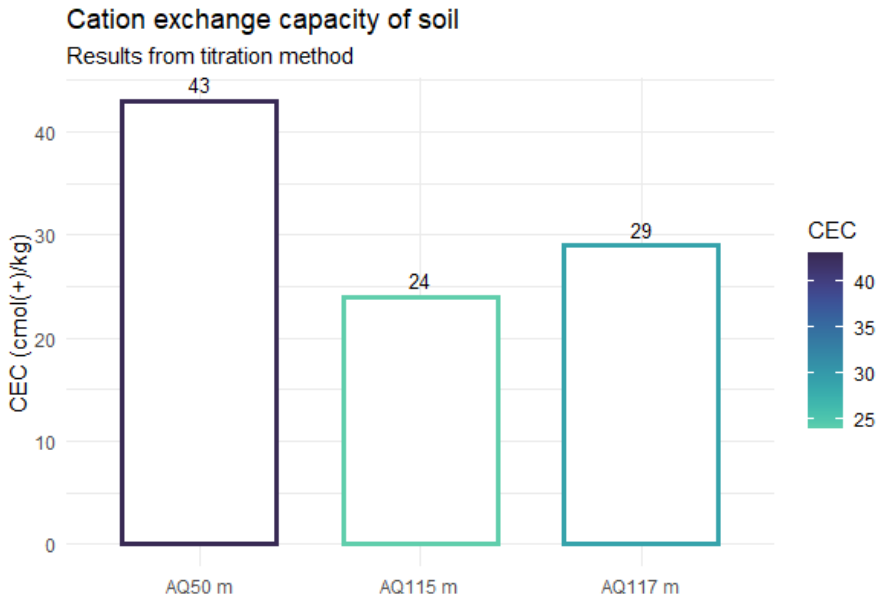

Figure 35. Graphical representation of the cation exchange capacity in the soil samples. Data are in cmol(+)·kg^{-1}. Colour is function of CEC value.

Table 11. Data about the cation exchange capacity value in the samples from AQ117 soil. Data are in cmol(+)·kg^{-1} and the uncertainty of the measures is reported.

Sample name	*CEC values (cmol(+)·kg^{-1})*
AQ117 I	37±1
AQ117 II	26±3
AQ117 III	24±9
AQ117 m	*29*±17

The titration method is the standard procedure for assessing the cation exchange capacity of soils [27,39]. The alternative method proposed here is based on specific procedures for determining cations in aqueous extracts. Several ions were detected in the water extract solution by the instrument, but the results could not be compared with data from the standard method.

4. DISCUSSION: INTERACTIONS BETWEEN ARCHAEOLOGICAL GLASS AND SOIL

The archaeological glasses from the site of Aquileia have the typical Roman composition with high concentration of calcium and sodium and lower amounts of magnesium and potassium. Soda-lime-silica glasses are known to be the most durable among ancient glasses, nevertheless the fragments considered in this case study present highly corroded surfaces allowing to make hypotheses about the specific features of soil environment that brought to the observed damage.

Recent studies [2,5-6,13-14,18,26,30-31,35,42] have searched for the environmental features affecting the conservation of vitreous objects. One pivotal extrinsic factor is the pH of the soil [18,30,35,42]. The pH of the medium directly in contact with the buried glass causes surface corrosion, as most of the chemical decay processes involve the interaction of the H^+ and OH^- species with the silica network [13]. In the accelerated ageing tests brought by Palomar [30], isolated and interconnected fissures are generated in Roman type glass surface when exposed to acidic pH. The fissures do not grow into pits because of the silanol groups (-Si-OH) which are resistant to decay and protect the surface from further damage. On contrast, in basic and neutral soils the initial fissures grow into pits due to the continuous loss of matter from the matrix: the OH^- ions close to glass break the siloxane bonds thus accelerating the rate of pitting growth. The dissolution of glass matrix is associated to pH>9 [7,19] and the degradation occurred in the tested glasses proves that the pH locally increases at the glass/solution interface [30]. The increment of the pH level was verified also in other contexts [10,29,31].

The experimental results from this study provide evidence that the surface corrosion is related to the chemical and physical properties of the burial soils. Iridescence is the most evident degradation phenomenon present on the surface of archaeological glasses from the AQ50 soil and this correlation is reflected in numerous other samples found in this area, but not considered in this case study. The samples from other soils – AQ115 and AQ117 – have pitting as primary corrosion form. The distinction of glass fragments according to the morphology of the alteration finds a correlation in the properties of the environmental soils. The soil AQ50 is characterised by a slightly acidic pH, ranging between 7.5 and 5.4 and decreasing with depth. In the comparison it is distant from values of the AQ115 and AQ117 soils which are more alkaline (pH≥8). As discussed above, the pH level is strictly linked to the type of corrosion occurring on the glass surface. Assuming that the soil pH in the past has not changed much from the measured value – which stands to reason considering that the pH depends largely on the soil matrix and that the buffer capacity of soils is known [3,11,16] – the hypothesis is the following: in alkaline context the OH^- species attack the -Si-O-Si- bonds of the glass matrix leading to local formation of pits and craters. Instead, in acidic conditions the H^+ ions promote the leaching of alkalis cations and contribute to the formation of the silica gel layer on the surface [29-30]. This mechanism would explain the presence of a thick iridescent patina on the surfaces of glasses from AQ50 and the prevalence of pitting in the other fragments.

The surface of the samples 115 and 117 is marked by a diffused pitting. A recent research published by Palomar and Llorente [17] describes the formation of pits as natural consequence

of fissures. In contact with alkaline solution the glass surface develops fissures, then the basic species concentrate inside the fissures and the attack of water enlarges the fissure into growing pits. The pit growth slows as the concentration of basic species decreases when water enters. This interpretation explains the random distribution of pits on the surface.

Some differences can be noticed between the two samples 115 and 117. The pits on the sample 117 are deeper and some of them have the typical circular structure of the rings. Both samples are covered with the iridescent patina that is almost invisible in the sample 117, whereas in the sample 115 it can be noticed at naked eye.

Iridescence – as described by Emami *et al.* [10] – is an optical effect given by refraction of light at different angles from the surface of glass because of different constituents. It is generally referred to as a failure of crystalline composition. In fact, during the alteration process alkali ions migrate towards the surface transported by moisture. The patina is formed by the continuous deposition of ions within the corroded layers through evaporation of water, thus developing the foliated structure. The altered patina observed in the glass fragments, especially the one covering the sample 50, is composed of many overlapped layers manifesting the loss of alkali ions and the environmental conditions [18]. Besides the rainbow-like effect, the layers appear intrinsically blue, with colour changing in whitish and ochre in several areas. The patina is widely cracked and the crust tends to flake off. The characteristic fragility of the patina was observed by Dal Bianco *et al.* [6] while studying archaeological glasses from the *Iulia Felix* wreck. The layers have the tendency to peel off as consequence of dehydration: since laminae alternate with zones rich in water and silanol groups, as water evaporates the layers tend to detach. Considering the presence of water in burial context, it is possible that after being excavated the fragments have undergone to a similar mechanism. The results of the LA-ICP-MS and SEM-EDS analyses are consistent with the presence of a silica-rich gel layer on the glass surface as consequence of a strong ion leaching process [2,6,10,18,28-29]. In the sample 50, the patina is very thick mainly in one of the two sides of the fragment. The hypothesis is that the fragment is part of a glass vessel which content was left inside. During burial the vessel content underwent to some reactions that glued it on the glass wall. The mechanisms leading to the formation of iridescent patina took place and the result is an ultra-thick patina with different layers. This kind of mineralisation of the original content is faced in the study by Palamara *et al.* [28] where a vessel had developed a thicker corrosion in the inside due to the original content, successively identified as madder lake. This conclusion explains the reason why the patina varies in thickness in the areas of the same fragment and also the presence of the ochre layer on top of the others.

As regards the iridescent patina, further considerations should be made. Iridescence is visible under the microscope also on the surface of the samples 115 and 117. Beyond the variation in width, one main difference between the patinas is the colour. The intense blue in the sample 50 can be related to the metal cations present in the bulk glass and deposited on the surface during the formation of the crust. The pristine glass of the sample 50 is dark blue realised by adding cobalt to the original batch [7,19]. Moreover, the profile distribution obtained with LA-ICP-MS indicates that not only alkali and alkaline-earth ions are leached, but also heavy metals, which are likely to give particular shades to the patina. In this way the green sample 115 and the decoloured sample 117 have developed respectively a coloured patina and a transparent layer, despite showing similar rainbow-like effect. The study conducted by Doménech-Carbó *et al.* [9] relates the formation of laminated corrosion – the step leading to iridescence – to the presence of groundwaters rich in K and Ca consistently with the extensive use of lands for agriculture.

This fact would explain why the iridescence patina is detected in numerous fragments from the site near Aquileia.

The characterisation of the environmental soils pointed out some physico-chemical features that may have contributed to the observed glass corrosion. The prevalence of specific minerals allows to define the soils as calcareous – such as the soils AQ115 and AQ117– or as clayey – the AQ50 soil. This note reflects the distinction of the soils according to the pH level and the corresponding degradation occurred in buried glasses. In addition to that and to the pH level, which is the parameter more indicated in describing the capacity of the soil to corrode archaeological glasses, other extrinsic factors should be considered. The cation exchange capacity of soil defines the ion availability in the environmental context and it influences the pH [3,16,25]. The three soils under study have a high exchange capacity, but the greatest value is owned by the AQ50 soil. It is the only soil sample with acidic pH and its electrical conductivity reaches very high values in the deepest sampling level. Undoubtedly, these parameters together contribute to the corrosion of the buried glasses, but the grade of their impact is still difficult to assess. What can be noticed is that the soil having the most extreme conditions – the AQ50 soil – is the one whose buried glasses show the most advanced corrosion.

A final consideration deserves to be made. The environmental context in which glasses were discovered is peculiar. Glass objects were found on the surface of fields after the plough of the soil. It is likely that glasses were exposed to atmospheric agents and buried again many times before their discover, in a periodical cycle given by the ploughing of land. This condition needs to be considered while analysing the samples, even though it characterised only the last part of the finding life, because it could have impacted to some extent in the preservation of buried glasses. Moreover, there should be the awareness of the fact that soil studies describe the present-day conditions of the environment, hence hypothesis about the corrosion power of the burial context can be made assuming that the measured data are not far from the environmental situation of the past.

5. CONCLUSIONS AND FUTURE DEVELOPMENTS

The primary objective of this thesis project is the investigation of the interactions between ancient glasses and the soil where the findings were buried for centuries. A multi-analytical approach was designed for the aim. The typology and the extent of the deterioration in archaeological glasses are evaluated and the burial context of the site is characterised.

This case study investigates a limited number of severely corroded vitreous findings from the site near the ancient Roman city of Aquileia. Optical Microscopy and SEM-EDS are fundamental in assessing surface degradation of fragments. The analysis of the altered crust proceeds with LA-ICP-MS. Successive ablations allow to create 2D and 3D mappings and to study in detail the change in composition of the glass surface. The degradation unveiled in archaeological glasses is the result of their interaction with the environment, therefore a correlation between soil properties and glass decay is found. The multilayered iridescent patina has developed in archaeological glasses coming from the AQ50 soil, where the high concentration of H^+ ions has produced a strong ion depletion. Instead, the alkaline context found in the AQ115 and AQ117 soils has brought to advanced pitting. The AQ50 soil, that has the most extreme conditions, is the only made of clay, which means that the mineralogical composition is likely to have an impact on the preservation of ancient glasses.

Glass degradation is a complex combination of mechanisms, therefore the explanation discussed in this thesis cannot be considered complete. This research aims to be the forerunner of future studies and developments on this topic. The direct study of ancient Roman glasses allowed to confirm the shared information about the mechanisms of glass alteration, but new research is needed. First, the mineralogical and textural composition of soil and their impact in glass preservation should be studied in detail. Furthermore, the conclusions drawn here should be verified with a wider project involving numerous soil samples from distinct archaeological sites to investigate the correlations from a statistical point of view.

6. REFERENCES

[1] Agilent, Ed., *Microwave Plasma Atomic Emission Spectroscopy (MP-AES). Application eHandbook*, 2021. Accessed: Feb. 09, 2022. [Online]. Available: https://www.agilent.com/cs/library/applications/5991-7282EN_MP-AES-eBook.pdf.

[2] Bertoncello R., Milanese L., Sada C., *Alteration and corrosion phenomena in Roman submerged glass fragments*, *Journal of Non-Crystalline Solids*, vol. 337, no. 2, pp. 136–141, 2004. doi: 10.1016/j.jnoncrysol.2004.03.118.

[3] Brady N.C., *The nature and properties of soils*, 9th ed., Macmillan Publishing Company, a division of Macmillan. Inc., 1984.

[4] Carmona N., García-Heras M., Gil C., Villegas M.A., *Chemical degradation of glasses under simulated marine medium*, *Materials Chemistry and Physics*, vol. 94, no. 1, pp. 92–102, 2005. doi: 10.1016/j.matchemphys.2005.04.026.

[5] Cox G.A., Ford B.A., *The long-term corrosion of glass by ground-water*, *Journal of Materials Science*, vol. 28, pp. 5637-5647, 1993.

[6] Dal Bianco B., Bertoncello R., Milanese L., Barison S., *Surface study of water influence on chemical corrosion of Roman glass*, *Surface Engineering*, vol. 21, no. 5–6, pp. 393–396, 2005. doi: 10.1179/174329305X64376.

[7] Davison S., *Conservation and Restoration of Glass*, Second Edition, Oxford: Butterworth-Heineman, Elsevier, 2003.

[8] Degryse P., Scott R.B., Brems D., *The archaeometry of ancient glassmaking: reconstructing ancient technology and the trade of raw materials*, *Perspective*, no. 2, pp. 224–238, 2014. doi: 10.4000/perspective.5617.

[9] Doménech-Carbó M.T., Doménech-Carbó A., Osete-Cortina L., Saurí-Peris M. C., *A study on corrosion processes of archaeological glass from the Valencian Region (Spain) and its consolidation treatment*, *Microchimica Acta*, vol. 154, no. 1–2, pp. 123–142, 2006. doi: 10.1007/s00604-005-0472-y.

[10] Emami M., Nekouei S., Ahmadi H., Pritzel C., Trettin R., *Iridescence in Ancient Glass: A Morphological and Chemical Investigation*, *International Journal of Applied Glass Science*, vol. 7, no. 1, pp. 59–68, 2016. doi: 10.1111/ijag.12182.

[11] Foth H.D., *Fundamentals of Soil Science*, 8th ed. John Wiley & Sons, Inc., 1990.

[12] Friedrich K.T., Degryse P., *Soil vs. glass: an integrated approach towards the characterization of soil as a burial environment for the glassware of Cucagna Castle (Friuli, Italy)*, *Science and Technology of Archaeological Research*, vol. 5, no. 2, pp. 138–156, 2019. doi: 10.1080/20548923.2019.1688492.

[13] Gin S., Delaye J.M., Angeli F., Schuller S., *Aqueous alteration of silicate glass: state of knowledge and perspectives*, *npj Materials Degradation*, vol. 5, no. 1, 2021. doi: 10.1038/s41529-021-00190-5.

[14] Gueli A.M., Pasquale S., Tanasi D., Hassam S., Lemasson Q., Moignard B., Pacheco C., Pichon L., Stella G., Politi G., *Weathering and deterioration of archeological glasses from late Roman Sicily*, *International Journal of Applied Glass Science*, vol. 11, no. 1, pp. 215–225, 2020. doi: 10.1111/ijag.14076.

[15] Hench L., *Glass surfaces*, *Journal de Physique Colloques*, vol. 43, no. C9, 1982. doi: 10.1051/jphyscol:19829125ï.

[16] Hillel D., *Environmental soil physics*. Academic Press. an Imprint of Elsevier, 1998.

[17] Jackson C.M., Greenfield D., Howie L.A., *An assessment of compositional and morphological changes in model archaeological glasses in an acid burial matrix*, *Archaeometry*, vol. 54, no. 3, pp. 489–507, 2012. doi: 10.1111/j.1475-4754.2011.00632.x.

[18] Jackson C.M., Greenfield D., Howie L.A., *An assessment of compositional and morphological changes in model archaeological glasses in an acid burial matrix*, *Archaeometry*, vol. 54, no. 3, pp. 489–507, 2012. doi: 10.1111/j.1475-4754.2011.00632.x.

[19] Janssens K., Ed., *Modern Methods for Analysing Archaeological and Historical Glass*, 1st ed. John Wiley & Sons, Ltd., 2013.

[20] Kibblewhite M., Tóth G., Hermann T., *Predicting the preservation of cultural artefacts and buried materials in soil*, *Science of the Total Environment*, vol. 529, pp. 249–263, 2015. doi: 10.1016/j.scitotenv.2015.04.036.

[21] Kurkjian C.R. and Prindle W.R., *Perspective on the history of glass composition*, *Journal of the American Ceramic Society*, vol. 81, no. 4, pp. 795–812, 1998.

[22] Lenting C., Plümper O., Kilburn M., Guagliardo P., Klinkenberg M., Geisler T., *Towards a unifying mechanistic model for silicate glass corrosion*, *npj Materials Degradation*, vol. 2, no. 1, 2018. doi: 10.1038/s41529-018-0048-z.

[23] Luckner K.T., *Ancient Art at The Art Institute of Chicago*, 1994.

[24] McBride M.B., *Environmental Chemistry of Soils*. New York, Oxford, Oxford University Press, 1994.

[25] Meetei T.T., Devi Y.B., Chanu T.T., *Ion Exchange: The Most Important Chemical Reaction on Earth after Photosynthesis*, *International Research Journal of Pure and Applied Chemistry*, pp. 31–42, 2020. doi: 10.9734/irjpac/2020/v21i630174.

[26] Melcher M., Wiesinger R., Schreiner M., *Degradation of glass artifacts: Application of modern surface analytical techniques*, *Accounts of Chemical Research*, vol. 43, no. 6, pp. 916–926, 2010. doi: 10.1021/ar9002009.

[27] Ministero delle Politiche Agricole e Forestali, International Union of Soil Sciences, Società Italiana della Scienza del Suolo, *Metodi di Analisi Chimica del Suolo*, Roma, Italy: Franco Angeli, 2000.

[28] Palamara E., Zacharias N., Papakosta L., Palles D., Kamitsos E. I., Pérez-Arantegui J., *Studying a Funerary Roman Vessel Glass Collection from Patras, Greece: An Interdisciplinary Characterisation and Use Study*, *Science and Technology of Archaeological Research*, vol. 2, no. 2, pp. 203–216, 2016. doi: 10.1080/20548923.2016.1239868.

[29] Palomar T., *Characterization of the alteration processes of historical glasses on the seabed*, *Materials Chemistry and Physics*, vol. 214, pp. 391–401, 2018. doi: 10.1016/j.matchemphys.2018.04.107.

[30] Palomar T., *Effect of soil pH on the degradation of silicate glasses*, *International Journal of Applied Glass Science*, vol. 8, no. 2, pp. 177–187, 2017. doi: 10.1111/ijag.12226.

[31] Palomar T., Llorente I., *Decay processes of silicate glasses in river and marine aquatic environments*, *Journal of Non-Crystalline Solids*, vol. 449, pp. 20–28, 2016. doi: 10.1016/j.jnoncrysol.2016.07.009.

[32] Panighello S., Šelih V.S., van Elteren J.T., Sommariva G., Orsega E.F., *Elemental mapping of polychrome ancient glasses by laser ablation ICP-MS and EPMA-WDS: a new approach to the study of elemental distribution and correlation*, *Integrated Approaches to the Study of Historical Glass*, vol. 8422, p. 842202, 2012. doi: 10.1117/12.975698.

[33] Panighello S., van Elteren J.T., Orsega E.F., Moretto L.M., *Laser ablation-ICP-MS depth profiling to study ancient glass surface degradation*, *Analytical and Bioanalytical Chemistry*, vol. 407, no. 12, pp. 3377–3391, 2015. doi: 10.1007/s00216-015-8568-7.

[34] Pansu M., Gautheyrou J., *Handbook of soil analysis: mineralogical, organic and inorganic methods*, Springer, 2006.

[35] Roemich H., Gerlach S., Mottner P., Mees F., Jacobs P., van Dyck D., Doménech-Carbó T., *Results from burial experiments with simulated medieval glasses*, *Materials Research Society Symposium Procedures,* vol. 757, 2003.

[36] Soil Science Division Staff, *Soil survey manual. USDA Handbook No. 18*. Washington, D.C.: Government Printing Office, 2017.

[37] Stuart B.H., *Analytical techniques in materials conservation*, John Wiley & Sons, Ltd., 2007.

[38] Tournié A., Ricciardi P., Colomban P., *Glass corrosion mechanisms: A multiscale analysis*, *Solid State Ionics*, vol. 179, no. 38, pp. 2142–2154, 2008. doi: 10.1016/j.ssi.2008.07.019.

[39] U. Nrcs Nssc Kssl, *Kellog Soil Survey Laboratory Methods Manual; Soil Survey Investigations Report No. 42*, Version 5.0, 2014.

[40] Van Giffen N.A.R., Koob S.P., *Deterioration of Vitreous Materials*, *The Encyclopedia of Archaeological Sciences*, John Wiley & Sons, Inc., 2018, pp. 1–4. doi: 10.1002/9781119188230.saseas0179.

[41] Weaver J.L., DePriest P.T., Plymale A.E., Pearce C.I., Arey B., Koestler R.J., *Microbial interactions with silicate glasses*, *npj Materials Degradation*, vol. 5, no. 1, 2021. doi: 10.1038/s41529-021-00153-w.

[42] Zacharias N., Palamara E., Kordali R., Muros V., *Archaeological glass corrosion studies: composition, environment and content*, *Scientific Culture*, vol. 6, no. 3, pp. 53–67, 2020. doi: 10.5281/zenodo.4007562.

[43] Zachariasen W.H., *The atomic arrangement in glass*, *Journal of the American Chemical Society*, vol. 54, no. 10, pp. 3841–3851, 1932. doi: 10.1021/ja01349a006.

7. SUPPLEMENTARY MATERIALS

Table S1. Values about the main elements in the soil samples. Data are in g·kg^{-1} and the uncertainty of the measures is reported. Cd, Co and Ni are under the detection limit of the instrument. Mn, Sr, Zn and Pb contents are smaller than 1 g·kg^{-1}. In some cases Pb content was under the detection limit.

Sample name	*Element content (g·kg^{-1})*							
	Al	*Ca*	*Cu*	*Fe*	*K*	*Mg*	*Na*	*Pb*
AQ50 I	34±1	12±1	<1	21±2	8±1	14±3	2.9±0.3	-
AQ50 II	34±1	13±1	<1	20±1	7.7±0.2	16±6	2.8±0.1	<1
AQ50 III	35±2	4.5±0.5	<1	20±1	8.0±0.2	15±1	2.9±0.1	-
AQ50 m	*35±1*	*10±12*	<1	*20±1*	*7.9±0.4*	*15±2*	*2.9±0.2*	-
AQ115 I	3±2	105±38	<1	<1	9±1	13±1	3.3±0.2	<1
AQ115 II	2±1	114±35	<1	<1	8±2	14±2	3.3±0.1	<1
AQ115 III	2.43±0.01	115±17	<1	23±1	9.5±0.2	13±2	3.5±0.2	<1
AQ115 m	*2.5±0.5*	*111±13*	<1	<1	*9±2*	*14±2*	*3.3±0.5*	<1
AQ117 I	2.9±0.4	105±6	5±3	47±3	12.9±0.3	2.3±0.2	4.8±0.1	2.1±0.1
AQ117 II	3±1	109±13	2.4±0.1	47±1	13.4±0.3	2.3±0.4	5±1	2±3
AQ117 III	2±1	109±5	<1	41±1	13±1	0.8±0.3	6.3±0.4	<1
AQ117 m	*3±1*	*108±6*	*3±5*	*45±5*	*13±1*	*2±2*	*5±2*	*2±2*

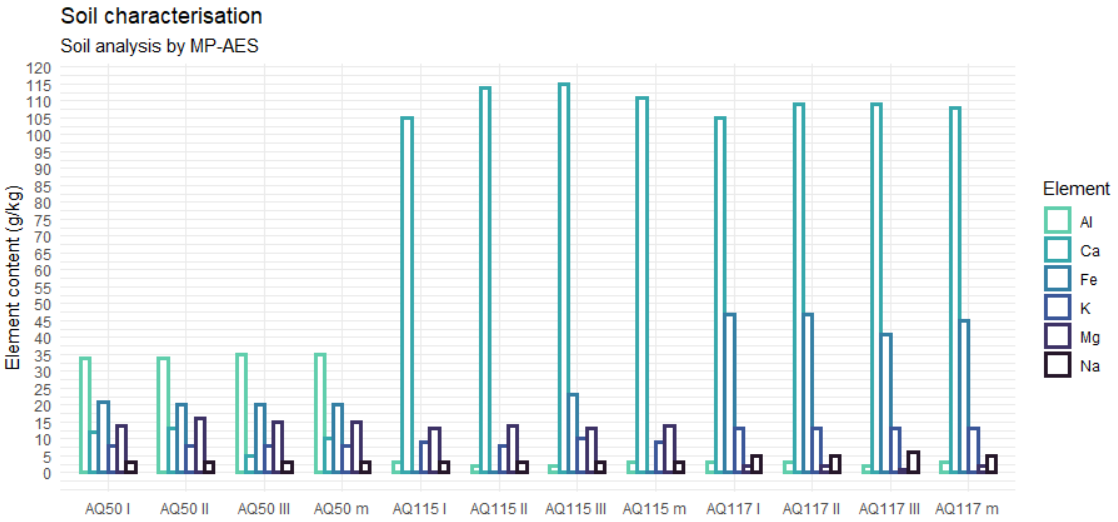

Figure S1. Graphical representation of data about the main elements in the soil samples. Data are in g·kg^{-1}. Colours identify different elements.

Table S2. Values about the pH in the soil samples. Data refer to the measures in saline solution and in aqueous solution. The uncertainty of the measures is ± 0.1 pH.

Sample name	*pH values*	
	$CaCl_2$ solution	*H_2O solution*
AQ50 I	7.5	7.8
AQ50 II	7.1	7.2
AQ50 III	5.4	5.4
AQ50 m	*6.7*	*6.8*
AQ115 I	7.9	8.4
AQ115 II	8.2	8.7
AQ115 III	8.2	8.7
AQ115 m	*8.1*	*8.6*
AQ117 I	8.0	8.4
AQ117 II	8.1	8.6
AQ117 III	8.1	8.5
AQ117 m	*8.1*	*8.5*

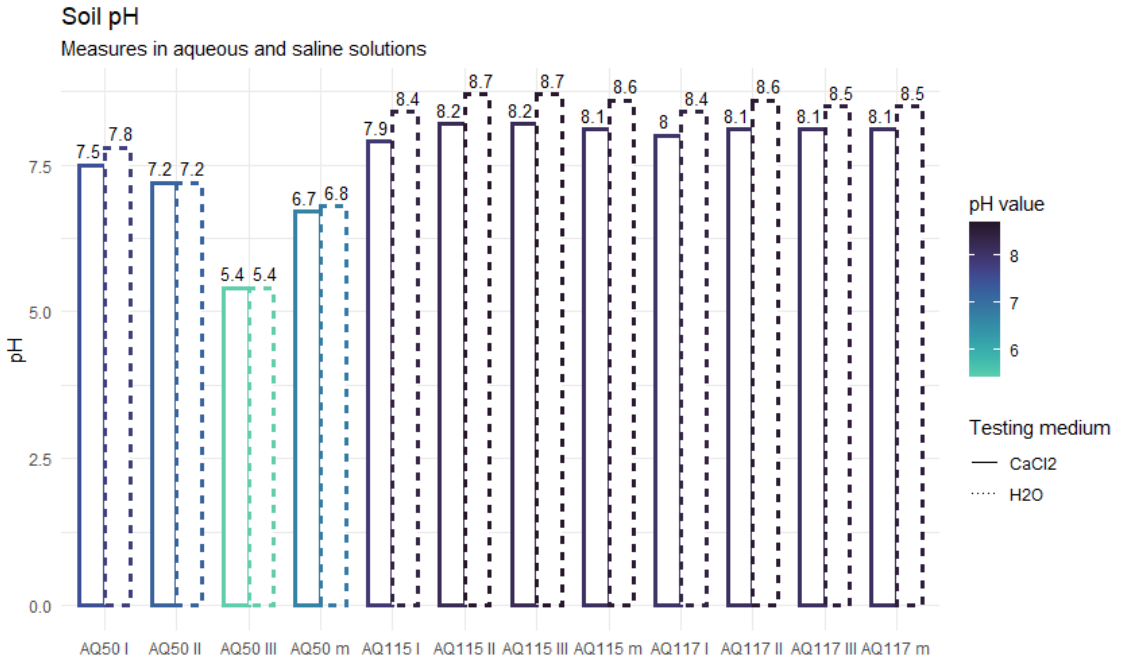

Figure S2. Graphical representation of the pH values in the soil samples. For each soil the value measured in two testing media is reported. Colour is function of pH level.

Table S3. Values about the cation exchange capacity in the soil samples. Data are in cmol(+)·kg^{-1} and the uncertainty of the measures is reported.

Sample name	*CEC values (cmol(+)·kg^{-1})*
AQ50 I	45±5
AQ50 II	43±2
AQ50 III	40±10
AQ50 m	*43*±7
AQ115 I	23.6±0.2
AQ115 II	24±5
AQ115 III	26±2
AQ115 m	*24*±3
AQ117 I	37±1
AQ117 II	26±3
AQ117 III	24±9
AQ117 m	*29*±17

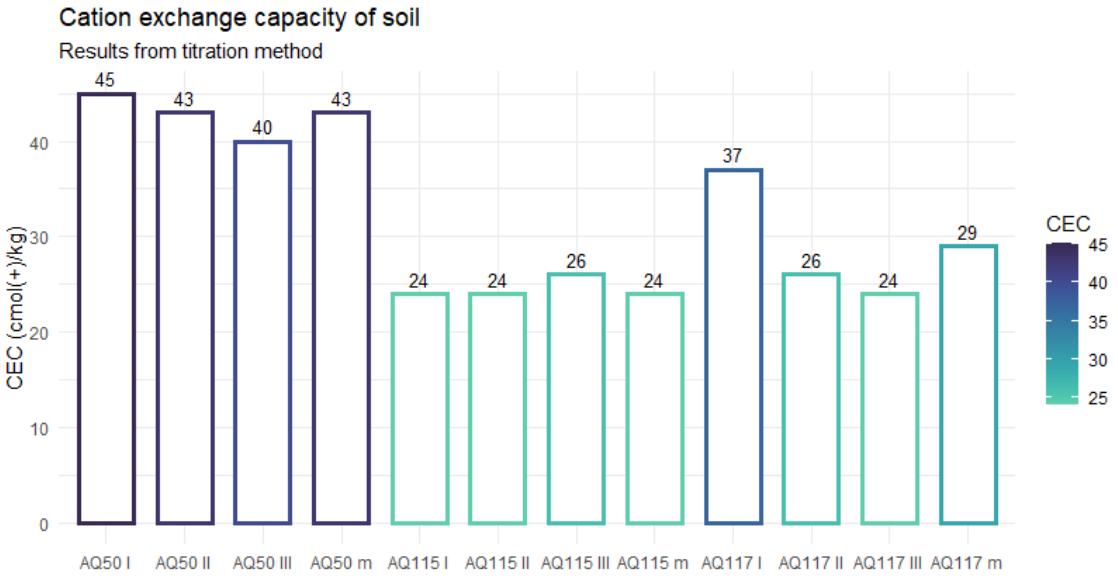

Figure S3. Graphical representation of the cation exchange capacity in the soil samples. Data are in cmol(+)·kg^{-1}. Colour is function of CEC level.

ACKNOWLEDGMENTS

I would like to thank Prof. Battistel for the availability, the patience, and the constant help he provided me during the writing of the thesis. I am grateful to Dr. Traviglia who gave me the chance to start the internship at the CCHT@CaFoscari facilities and develop the project in my final thesis. I thank Giulia Franceschin e Roberta Zanini for being my guides in this long collaboration. I would like to thank all the researchers and PhD students and all the other people I worked with for the help they gave me.

I thank *Soprintendenza Archeologia, Belle Arti e Paesaggio* of Friuli Venezia Giulia and *Museo Archeologico Nazionale* of Aquileia for allowing me to study the archaeological glasses and show them in my thesis.